Nousiainen, Olli, Characterization of reliable second level lead-free BGA interconnections in thermomechanically loaded LTCC/PWB assemblies

Department of the Mechanical Engineering, University of Oulu, P.O.Box 4200, FI-90014 University of Oulu, Finland

Abstract

Low-temperature co-fired ceramic (LTCC) based system-in-package (SiP) is an emerging multilayer module technology for wireless communication applications, mainly due to its excellent high-frequency material properties. The LTCC-SiP modules are typically soldered on an organic motherboard, but the lifetime of the 2nd level solder joints (i.e. the joints between platform and mother board) is often poor due to the high stress level of the joints in the test/field conditions. Moreover, applying of the lead-free solders in the interconnections of LTCC modules raises new questions about the feasibility and reliability of the solder joints in the LTCC applications. Therefore, the characteristic features of the reliable 2nd level solder joint configuration were determined in this thesis using non-destructive inspection (NDI) techniques, optical microscopy, and electronic microscopy. This will enable the electronics industry to fabricate reliable assemblies consisting of LTCC tapes with typical coefficient of thermal expansion (CTE) value, common printed wiring board (PWB) materials, and commercial solder joint materials.

It was proved that collapsible Sn4Ag0.5Cu (SAC405) spheres are not a feasible option the in the LTCC/PWB assemblies with large global thermal mismatch, but a non-collapsible ball grid array (BGA) joint with a plastic core solder ball (PCSB) was required for adequate reliability of such assemblies. The results also showed that intergranular (creep) cracking was the dominant failure mechanism of the lead-free non-collapsible BGA joint in the thermal cycling test (TCT) over a temperature range of 0 °C - 100 °C and the lifetime of the joints was increased compared with the similar joint configuration with lead containing solder. However, when the test assemblies were exposed into the harsher TCT over a temperature range of –40 °C - 125 °C, a mixed transgranular/intergranular failure and separation at the solder/IMC interface occurred primarily in the AgPt metallized LTCC modules with the BGAs containing ternary SAC solder. The reliability of these joint was also poorer compared with the lead containing joints. This problem was solved when a novel BGA joint configuration consisted of Sn7In4.1Ag0.5Cu solder and the PCSB was applied to the LTCC modules. Moreover, this thesis also proved that there is a relation between the primary failure mechanisms of the various Sn based lead-free solders and thermomechanically induced stress level in the present non-collapsible BGA joint configuration.

Finally, the effect of the deposit material of the solder lands on the failure mechanism of the BGA joints in the LTCC/PWB assemblies was studied. The results showed that the adverse phenomena related to the sintered Ag based metallization materials can be avoided using electroless nickel with immersion gold (ENIG) as a deposit material. On the other hand, this study also demonstrated that the inadequate adhesion strength of the commercial base metallization in the ENIG plated modules resulted in the disadvantageous failure mechanism of the test assemblies. Therefore, the criteria for the material selection and the design aspects of the reliable 2nd level interconnection were discussed thoroughly in this thesis.

Keywords: creep, lead-free solders, low-temperature co-fired ceramic, plastic-core solder balls, therrmal fatigue

List of abbreviations and symbols

β	Weibull's shape factor
θ	Characteristic lifetime
ΔK	stress intensity factor
3D	three-dimensional
BGA	Ball Grid Array
CBGA	Ceramic BGA
CCGA	Ceramic Coumn Grid Array
CGA	Column Grid Array
CSL	Coincidence Site Lattice
CSP	Chip Scale Package
CTE	Coefficient of Thermal Expansion
DC	Direct Current
DNP	Distance to Neutral Point
EDS	Energy Dispersive Spectrometry
ENIG	Electroless Nickel Immersion Gold
$F^{\#}$	Degree of focusing
FE-SEM	Field Emission Scanning Electron Microscope
H	Height
HTCC	High-Temperature Co-fired Ceramic
IMC	Intermetallic Compound
L	Length
LTCC	Low Temperature Co-fired Ceramic
LGA	Land Grid Array
NDI	Non-Destructive Inspection
OIM	Orientation Imaging Microscopy
PBGA	Plastic BGA
PCSB	Plastic-Core Solder Ball
PWB	Printed Wiring Board
Q_{core}	Activation energy for core-diffusion-controlled dislocation climb
RoHS	Restriction of Hazardous Substances
RF	Radio Frequency
RT	Room Temperature
SAC	SnAgCu alloys
SiP	System-in-Package
SMT	Surface-Mount Technology
SAM	Scanning Acoustic Microscope
SEM	Scanning Electron Microscope
TCT	Thermal Cycling Test
V	Volume
W	Width

List of original papers

I Nousiainen O, Putaala J, Kangasvieri T, Rautioaho R & Vähäkangas J (2007) Failure mechanisms of thermomechanically loaded SAC/PCSB joints in LTCC/PWB assemblies. Journal of Electronics Materials 36(3): 232 - 241.

II Nousiainen O, Kangasvieri T, Rautioaho R & Vähäkangas J (2008) Effect of Sn7In4.1Ag0.5Cu solder on the thermal fatigue of lead-free composite solder joints in LTCC/PWB assemblies. Soldering & Surface Mount Technology 20(3): 11 - 17.

III Nousiainen, O., Lehtiniemi, L., Kangasvieri, T., Rautioaho, R & Vähäkangas J (2008) Thermal fatigue endurance of collapsible 95.5Sn4Ag0.5Cu spheres in LTCC/PWB assemblies. Microelectronics Reliability 48(4): 622 - 630.

IV Nousiainen O, Kangasvieri T, Rautioaho R & Vähäkangas J (2009) Thermal fatigue endurance of lead-free composite solder joints over a temperature range of –55 °C - 150 °C. Journal of Electronics Materials 38(6): 843 - 851.

V Nousiainen O, Kangasvieri T, Kautio K, Rautioaho R & Vähäkangas J (2010) Effect of electroless NiAu deposit on reliability of thermomechanically loaded lead-free composite joints in LTCC/PWB assemblies. Soldering & Surface Mount Technology 22(x):

Paper I investigates thermal fatigue endurance of a lead-free BGA solder joint configuration with Sn4Ag0.5Cu (SAC405) solder and plastic-core solder balls in LTCC/PWB assemblies. The results show that the thermal fatigue endurance of the joint is not as good as it has been in the similar test assembly with Sn36Pb2Ag solder in the thermal cycling test over a temperature range of –40 °C - 125 °C. In this test conditions, two independent primary cracks were induced at the temperature extremes: 1) A mixed fatigue/creep failure at the low temperature (–40 °C) and 2) a failure at the solder/intermetallic compound (IMC) interface at the high temperature (125 °C). In the milder TCT (0 °C - 100 °C), the intergranular (creep) cracking was the dominant failure mechanism of the joint.

Paper II presents the implementation of the Sn7In4.1Ag0.5Cu solder (SAC-In) in LTCC/PWB assemblies. As an outcome, a novel lead-free non-collapsible BGA joint configuration with enhanced thermal fatigue endurance in two thermal cycling conditions (0 °C - 100 °C and –40 °C - 125 °C) is presented. Moreover, different primary failure mechanism (creep) in the harsh TCT (–40 °C - 125 °C) was observed compared with the SAC405/PCSB/SAC405 joints.

Paper III investigates the thermal fatigue endurance of SAC405 solder spheres in LTCC/PWB assemblies by varying the temperature swing of the thermal cycling tests and the global thermal mismatch of the test assemblies. The results proved that the SAC405 spheres are not a feasible option for the 2nd level interconnections in the LTCC/PWB assemblies with large global thermal mismatch. Moreover, the results showed that decreasing the global thermal mismatch of this joint configuration changed

the failure mechanism of crack formed at the low (-40°C) temperature extreme from transgranular (fatigue) to intergranular (creep).

Paper IV shows that the primary failure mechanism of SAC-In joints changed from creep to mixed fatigue/creep failure at the low (–55 °C) temperature extreme in the severe thermal cycling conditions. However, notable enhancement in the thermal fatigue endurance of the solder joint configuration was achieved using the indium containing solder, since the characteristic lifetime of the SAC-In joints was 75 % higher compared with the SAC405 joints.

Paper V presents the effect of the metallization material on the failure mechanisms of the thermomechanically loaded non-collapsible solder joint configuration in LTCC/PWB assemblies. The results indicate that the separation between the IMC layer and solder matrix can be avoided using ENIG deposit, but the thermal fatigue endurance of the lead-free solder had the major effect on the characteristic lifetime instead of the deposit material of the solder land. Finally, the requirements of the reliable solder joint configuration in LTCC/PWB assemblies are discussed.

The test assemblies and the experiments of the Papers I - V were planned by the author and Dr. Tero Kangasvieri. The author prepared the drafts of the original papers and, subsequently, wrote the final versions in respect of the co-authors' comments. The accelerated testing, non-destructive investigations, and metallographic examinations presented in the studies were conducted or supervised by the author. The LTCC modules were fabricated by VTT Electronics, Selmic, and EMPART research group. The ENIG deposit of the test modules were plated by Atotech Gbhm. All test assemblies were manufactured in Microelectronics and Material Physics laboratories by Dr. Tero Kangasvieri, Mr. Jussi Putaala, Mr. Lauri Lehtiniemi, Mr. Timo Urhonen, and the author.

Contents

1 Introduction

Due to its excellent high-frequency material properties (low loss and dispersion) and its dense 3D integration and miniaturization capability, multilayer low-temperature co-fired ceramic (LTCC) is a highly viable substrate platform for highly-integrated microwave and millimeter-wave System-in-Packages (SiPs) for automotive, wireless communication and industrial automation applications [1-3]. These applications are typically mounted and soldered onto a printed wiring board (PWB). However, the life-time of the 2nd level solder joints (i.e. the joints between platform and mother board) is often poor due to the high stress level of the joints in the test/field conditions, since the global thermal mismatch between most LTCC tape systems and printed wiring boards is usually more than 10 ppm/°C [4-6]. Also the flexural strength of LTCC material is low compared with high-temperature co-fired ceramic (HTCC) materials [7]. Therefore, the thermomechanically loaded LTCC packages are more prone to the ceramic cracking compared with the HTCC packages. On the basis of the observations reported literature [5,8-11], the thermomechanically induced failures in the LTCC joint configurations can be classified as follows:

Type I: Cracking within ceramic
Type II: Cracking at the ceramic/metallization interface
Type III: Cracking within solder
Type IV: Cracking within the non-collapsible sphere

The excessive reaction between liquid solder and solid metallization during soldering process causes usually the type I failures. In this case, the strength and elastic modulus of the solder region next to the ceramic interface is increased by dispersion hardening due to the formation of the numerous intermetallic compounds (IMC) particles within the solder joint. This induces cracks to propagate in the LTCC ceramic instead of in the solder region [9,12-15]. In failures of type II, the pad metallization detaches from the LTCC substrate during thermal cyclic loading due to inadequate adhesion between metallization and LTCC or the crack initiates and propagates along the mixed zone (i.e. the narrow zone containing both ceramic and metallic particles) [8,13]. Type III represents cracking in the solder near the solder lands of the test assembly. This failure type is considered to be the preferred failure type, since this failure can be detected using DC measurements and the life-time of the joint may be estimated with reasonable accuracy, which is not possible with the other failure types [5,15]. Type IV failure exists in the non-collapsible BGA joints. It is related to the high shear stress distribution in the middle of the non-collapsible sphere [16].

Generally, the occurrence of failure types I, II and IV may be avoided by reducing the global thermal mismatch between the LTCC and PWB base materials. This is also an effective way to enhance the lifetime duration of LTCC/PWB assemblies [17]. However, PWB materials with low coefficient of thermal expansion (CTE) values are more expensive than standard FR-4. On the other hand, increasing the CTE of the LTCC material may induce a larger thermal strain into the possible first level interconnections of LTCC applications. The number of suppliers of LTCC materials with the high CTE values is

also limited. Thus, designing a robust and reliable 2nd level solder joint configuration seems to be reasonable, since it enables to fabricate assemblies consisting of LTCC tapes with typical CTE value and common PWB materials.

Besides the reliability problems due to large global thermal mismatch between LTCC and PWB, the applying of the lead-free solders in the interconnections of LTCC modules raises new problems. First, it has been predicted that the use of lead-free solder causes more severe dissolution of thick film metallizations during soldering due to the higher temperatures required in soldering and the higher tin content of the lead-free solders [18]. Furthermore, the thermal fatigue endurance of lead-free solders vary in the different component packages and thermal cycling conditions compared with the SnPb(Ag) solders resulting in the inadequate life-time of thermomechanically loaded lead-free solder joints in some cases [19-23].

1.1 Solder joints configurations in LTCC/PWB assemblies

1.1.1 Joint types

Considering that the surface mount technology (SMT) is the main fabrication method of LTCC/PWB assemblies, LTCC-SiP modules can be soldered to a PWB using a ball grid array (BGA), land grid array (LGA) or column grid array (CGA) joints.

Two different BGA joint types are used in SMT. In a non-collapsible BGA joint, a sphere, which does not melt during the soldering, is used to guarantee sufficient BGA joint stand-off height. Two practical options are available for the selection of the non-collapsible sphere, namely 90Pb10Sn spheres and plastic-core solder balls (PCSB). However, it has been shown that the reliability of non-collapsible 90Pb10Sn/lead-free solder joints in a RoHS compatible LTCC/PWB assembly is insufficient due to the excessive dissolution of lead into liquid solder during the reflow soldering [24].

Okinaga et al. [16] has introduced plastic core solder balls (PCSB) as an alternative choice for 90Pb10Sn spheres. The plastic core with low Young's modulus is aimed for relaxing thermally induced stresses in BGA solder joints. The PCSBs can also provide predicTable RF characteristics since they maintain their stand-off height during board-level assembly. Furthermore, in-house as well as by conducted full-wave electromagnetic simulations have clearly shown that the polymer core has no significant degrading impact on RF/microwave performance of the BGA package [8, 25]. The changes in thermal performance of the PCSB are also small compared with a eutectic BGA solder joints [26]. However, the number of commercial manufacturers of PCSBs is limited at the present moment.

A collapsible lead-free solder sphere is one possible choice for the second-level joints of ceramic BGA packages. Farooq et al. [27] used a thermal cycling test over the temperature range of 0 °C-100 °C to investigate the thermal fatigue of single-melt SAC spheres and 90Pb10Sn/63Sn37Pb non-collapsible solder joints in ceramic BGA/FR-4 assemblies.

The results showed that the SnAgCu spheres had almost twice the fatigue life of the lead-containing composite joints, despite the noticeably smaller (1:2) stand-off height of the SAC spheres. Thus, the collapsible lead-free solder sphere might be feasible solution also in LTCC technology.

LGA solder joints have a few advantages compared with BGA joints, which can be listed as follows: 1) lack of solder ball attachment, 2) lower stand-off height, 3) capability of finer pitch design, and 4) cost-effectiveness due to a smaller amount of solder [28]. In the case of LTCC applications, it has been shown that the characteristic lifetime of the thermomechanically loaded LTCC/PWB assemblies with a high global thermal mismatch (> 10 °C/ppm) remains at an inadequate level [29]. This limits the feasibility of the LGA joints in the LTCC applications.

In order to enhance the reliability of the 2nd level solder joints in ceramic packages, a column grid array (CGA) interconnection method can be used. An extensive study on thermomechanically loaded ceramic CGA (CCGA) packages tested in harsh test conditions was published earlier [30]. The column materials used in CCGA packages are either 90Pb10Sn alloy or copper. High-lead 90Pb10Sn columns are currently exempted from RoHS legislation and, therefore, they can be used in lead-free assemblies [31]. However, severe Pb dissolution from solid 90Pb10Sn solder to liquid lead-free Sn-based solder occurs during the soldering process. The Pb dissolution may significantly decrease the lifetime duration of these solder joints [32], like it does in the case of non-collapsible 90Pb10Sn/SnAgCu non-collapsible solder joints in LTCC/PWB assemblies [24]. In lead-free applications the columns are either 90Pb10Sn alloy wrapped with copper or thin (250 μm) Cu columns [30,32-34]. Unfortunately, the thin columns are difficult to process, since they bend easily and require special tooling [25].

1.1.2 Solder lands and solders

The thick film printed solder lands of a LTCC module are often fabricated using Ag or Ag-based metallization emulsions. It has been shown that Ag-based metallizations (AgPd and AgPt) react with tin faster than silver [35]. Especially, it has been suggested recently that AgPd metallization may be used in lead-free 1st level interconnections between silicon chips and the LTCC substrate [36], but it must be noted that this metallization material is not feasible for 2nd level solder joints between the substrate and the organic motherboard (PWB) due to its tendency to dissolve into molten solder [9,11-15,37]. The formation of the Ag_3Sn and $AgPd_4$ causes dispersion strengthening in the solder matrix, which, in turn, induces ceramic cracking in the thermomechanically loaded LTCC substrate, as mentioned before.

The quality of the metallization also affects the dissolution rate of the metallized solder lands. The roughness and porosity of the thick film increases the effective area between liquid solder and solid LTCC metallization and, consequently, results in faster dissolution of the initial metallization layer during the soldering process. This is due to the fact that dissolution at the solid/liquid interface is governed by the surface area of the solid and the

volume of the liquid. The roughness of fired metallization naturally increases the surface area of the solder lands and in a porous metallization layer liquid solder will flow into the pores due to capillary force resulting in more contact area between liquid solder and solid metallization [18,38,39]. This may also result in the excessive dissolution of a Ag-based metallization and degraded reliability, as was in the case of LTCC modules with Ag2.5Pt [40]. Furthermore, the sintered Ag-based metallization thick films also contain a certain amount of glass phase, which may deteriorate the wettability of the solder lands [41]. A post-processed deposit layer is a useful solution to avoid the above-mentioned problems. Therefore, an ENIG surface finish has been used in LTCC packages [17].

The importance of sufficient adhesion between LTCC and metallization is also crucial to the reliability of the solder joints of LTCC modules in order to avoid the failure type II. It has also been shown earlier that a solder mask was required in LTCC/PWB assemblies with a large global thermal mismatch in order to diminish the occurrence of the failure types I and II [5,15,42]. The size of the solder land area of the LTCC module can be increased in order to enhance the adhesion strength of the interface. This creates more beneficial stress distribution at the edge of the solder land. Another point is to increase the yield of the LTCC modules due to the wider tolerances in solder mask alignment during the printing process.

The selection of the solder material is obviously one of the key factors considering the thermal fatigue endurance of the critical regions of the solder joint (i.e. the location of high strain energy density). Hwang has listed the low-cycle fatigue life of numerous solder materials, from binary to pentanary and higher-element alloys [43]. Although these results the above-mentioned data are indicative for material selection process, they do not necessarily correlate with the thermal fatigue endurance of actual solder joints. Therefore, numerous studies focusing on the shear strength and/or creep resistance of the different solder joints in isothermal test conditions have been conducted. Unfortunately, these results of these tests do not always correspond to the thermal fatigue endurance of the real solder joints, since the weakest part of the joint in isothermal tests does not necessarily exist in the same location of the thermomechanically loaded joint due to the temperature dependent properties of the materials and the metallurgical phenomenon (recrystallization, solid-state phase transformations and coarsening of the IMC paricles) occurring in the solder joint.

It is also generally known that the creep/fatigue resistance of a solder joint is highly dependent on the actual distribution of thermally induced stresses in the joint and the other mechanical properties of the joint (strength, plasticity and Young's modulus) depend on temperature. Consequently, the solder material, which is suiTable for one electronic package type in the certain conditions, might have inadequate thermal fatigue endurance in another package type in the same test conditions. Therefore, the solder joint configurations used in other electronic packages (e.g. CSP, PBGA, CBGA, etc.) might be useless in LTCC applications.

1.2 Aim of the study

For abovementioned reasons and due to the lack of a fundamental study concerning the reliability of lead-free solder joints in LTCC applications, there is an obvious interest in designing and characterizing a feasible and reliable second-level joint configuration for lead-free LTCC/PWB assemblies. Therefore, the aim of this study is to characterize the features of a reliable 2nd level solder joint configuration in order to fabricate assemblies consisting of LTCC tapes with typical CTE value, common PWB materials, and commercial solder joint materials. The requirements for such joint configuration can be listed as follows:

1. The characteristic lifetime of the joint configuration has to match the standard requirements of the typical test conditions of the surface mount devices [44].

2. The primary failure must be located within the solder matrix and it should be preferably related to the creep cracking. This enables the reasonable lifetime estimation of the joint using either FE modeling or analytical models.

3. In the perspective of industrial manufacturers, it is essential that the joint configuration can be fabricated using the common processes of SMT.

The main focus of this thesis is directed to the effect of thermal loading on the failure mechanism of completely lead-free composite joints in an LTCC/PWB assemblies with high (> 10 ppm/°C) global thermal mismatch. The characteristic metallurgical features and the effect of thermal loading conditions on the failure mechanism of the joint configurations in various LTCC/PWB assemblies are investigated. Finally, the relation between the failure mechanisms and characteristic lifetime is discussed and the design aspects of the reliable 2nd level interconnection are given.

2 Experimental procedures

2.1 Test assemblies

2.1.1 Modules with non-collapsible BGA joints

The Sn4Ag0.5Cu (SAC405) solder with PCSB was used on the first lead-free solder joint configurations in order to clarify the behaviour of a common hypereutectic SAC alloy in the thermomechanically loaded LTCC/PWB assembly. The behaviour of eutectic Sn3.8Ag0.7Cu (SAC387) was tested in two test sets with the ENIG deposited metallization.

Considering the improvement in the thermal fatigue durability of the critical regions of the composite solder joint (i.e. the edges of the joint on the LTCC side), the quaternary Sn7In4.1Ag0.5Cu (SAC-In) alloy was used in this study. The SAC405solder was used on the PWB side of these test joints for two reasons. Firstly, its creep/fatigue properties were assumed to be sufficient, since no major failures have been found on the PWB side of the non-collapsible joint consisting of SAC405 solder with PCSB [Paper I]. This configuration also enables the use of the SnAgCu alloys in the solder joints of the other components to be soldered on the PWB in industrial assemblies. Thus, the use of the more expensive indium containing alloys can be minimized.

The test modules of test assemblies A - C were fabricated using the Dupont 951 material system with co-fired thick-film conductors the modules of test assembly D were fabricated using the Clad CT800/HL2000 material system with thick-film conductors. ENIG deposition of the test assemblies C and D was fabricated by Atotech GmbH. The solder paste was printed onto the pads of the test modules using a 180-μm-thick stencil, PCSBs were place on the pads, and the modules were subsequently soldered in a reflow oven. After the first reflow route, the solder paste was printed on the PWBs using a 150-μm-thick stencil and the assemblies were soldered after the placing the module onto them.

A schematic presentation of the non-collapsible interconnection is shown in Fig. 1. The main dimension and the materials of the test sets are given in Tables 1 and 2. Note that the thickness of the ENIG plated DuPont 951 modules is 1.2 mm instead of 1.0 mm presented in Paper V.

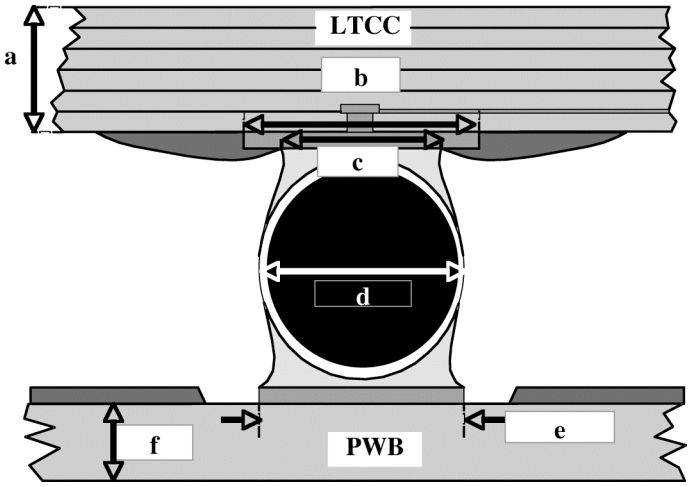

Fig. 1. A schematic presentation of the non-collapsible joint configuration.

Table 1. Dimension of the test assemblies with non-collapsible joints.

Assembly	LTCC	a (mm)	b (mm)	c (μm)	d (μm)	e (μm)	f (mm)	reference
A	DuPont 951	1.0	1.0	800 ± 30	800	650 ± 30	1.6	Papers I and II
B	DuPont 951	1.0	1.0	800 ± 30	1100	650 ± 30	1.6	Paper IV
C	DuPont 951	1.2	1.0	800 ± 30	800	650 ± 30	1.6	Paper V
D	HL2000/CT800	0.7	1.2	800 ± 30	800	650 ± 30	1.6	Paper V

Table 2. Materials of the test joints with PCSBs.

Joint	LTCC tape system	Solder on the LTCC side of the module	Metallization of LTCC	Reference
SAC405	Dupont 951	Sn4Ag0.5Cu	AgPt (QS264)	Papers I and IV
SAC-In	Dupont 951	Sn7In4.1Ag0.5Cu	AgPt (QS264)	Papers II and IV
E-SAC387	Dupont 951	Sn3.8Ag0.7Cu	Ag (Du Pont 6154)+ENIG	Paper V
E-SAC-In	Dupont 951	Sn7In4.1Ag0.5Cu	Ag (Du Pont 6154)+ENIG	Paper V
H-SAC387	Heralock	Sn3.8Ag0.7Cu	Ag (Heraeus LPA405-067)+ ENIG	Paper V
H-SAC-In	Heralock	Sn7In4.1Ag0.5Cu	Ag (Heraeus LPA405-067)+ ENIG	Paper V

The peak temperatures and the times above liquidus of the SAC405, SAC387, and SAC-In joints are given in Table 3. It must be noted that the profile used in the 2nd reflow resulted in 60 seconds above the liquidus temperature of SAC-In. The profiles were measured for Dupont 951 modules. It was assumed that the differences in thermal mass and heat conductivity between test assemblies were negligible. A SIKAMA Falcon 5C convection/conduction reflow oven was used in every case.

Table 3. Reflow parameters of the test assemblies.

1st reflow	**Time above liquidus (s)**	**Peak temperature (°C)**
SAC405 modules	45	231
SAC387 modules	51	236
SAC-In modules	70	225
2nd reflow	**Time above liquidus**	**Peak temperature**
SAC405	40	232

2.1.2 Modules with collapsible BGA joints

The test modules were fabricated using a standard multilayer LTCC process. The 15 mm x 15 mm LTCC modules had BGA connections in a 9x9 matrix with a 1.5 mm pitch. The overall thickness of the LTCC substrate was 1.2 mm. The two outermost BGA rows were daisy-chained. A solder mask was screen-printed with a co-firing process. The pad metallization of the LTCC substrate was composed of AgPt (DuPont Qs 264). A water-soluble flux was screen-printed onto the LTCC pad metallization. Solder balls were attached to the LTCC substrate by placing 0.762mm diameter 95.5Sn4Ag0.5Cu solder balls on the BGA pads and soldering them at peak temperatures of 240 °C - 252 °C. The test modules were soldered to four PWBs, each capable of encompassing 9 modules. The average stand-off height of the joints was 0.45 mm. The area array of a test module and a joint configuration are shown in Fig. 2 and the stencil sizes and material compositions can be found in Table 4.

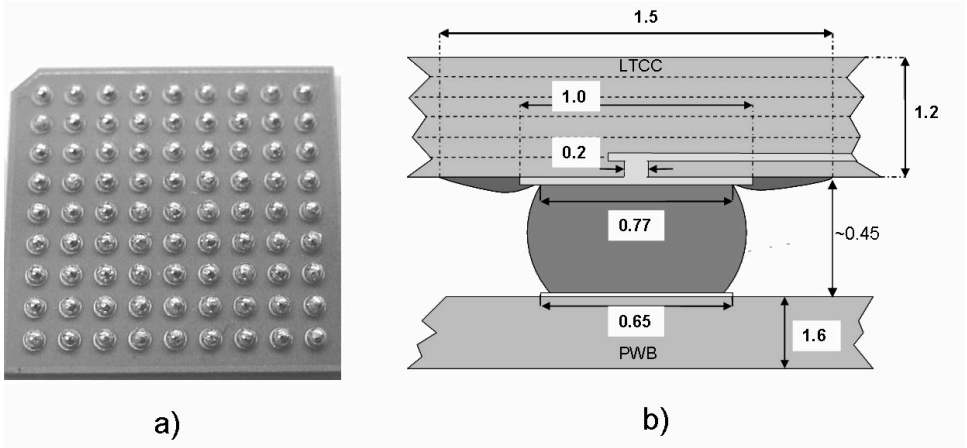

Fig 2. a) A test module after the ball attachment and b) schematic presentation of the test structure and its dimensions in mm (not to scale) [Paper III].

Table 4. Main specifications of the test structure [Paper III].

MODULE	
LTCC green tape system	Du Pont 951 PX™
CTE of LTCC	5.8 ppm/°C
Dimensions (mm)	15 x 15 x 1.2 (W x L x H)
Ball Grid Array and pitch (mm)	9x9 matrix, 1.5
Inner conductor material	Ag (Du Pont 6142)
Via material	Ag (Du Pont NO55)
Pad material	99/1 AgPt (Du Pont QS 264)
Solder mask material	post-fired glass (Du Pont 9615)
JOINT	
solder	Alpha OM-338 (95.5Sn4Ag0.5Cu)
Non-collapsible sphere	Sekisui SOL (PCSB, ∅ = 800 μm)
Stencil, module side	Thickness 180 μm, apertures 875 μm
Stencil, PWB side	Thickness 150 μm, apertures 720 μm
PWB	
FR-4 (PCL-FR-370)	thickness = 1.6 mm, CTE = 15 ppm/°C
Arlon 55NT	thickness = 1.6 mm, CTE = 9 ppm/°C
Cu-pad deposit	ENIG (electroless Ni/Au)

2.2 Thermal cycling tests

In the thermal cycling tests, test boards were exposed to 24 cycles per day. A fifteen-minute dwell time at the temperature extremes was applied in the tests to allow creep/stress relaxation. The complete test program and the number of the tested modules in the certain test condition are given in Table 5. The TCTs was based on the guidelines of JEDEC Standard No. 22-A104C [45]. Resistance changes in the daisy-chained test assemblies were monitored using a Fluke 2635A data logger. Since a continuous resistance measurement cannot be made with the data logger, a test module was defined as being damaged when its initial resistance of ≈ 1.5 Ω doubled.

Table 5. Test sets.

Assembly	Test joint	Number of modules	TCT	Reference
A	SAC405	9	0 °C - 100 °C	Paper I
A	SAC405	27	−40 °C - 125 °C	Paper I
A	SAC-In	18	0 °C - 100 °C	Paper II
A	SAC-In	18	−40 °C - 125 °C	Paper II
B	SAC405	9	−55 °C - 150 °C	Paper IV
B	SAC-In	9	−55 °C - 150 °C	Paper IV
C	E-SAC387	9	−40 °C - 125 °C	Paper V
C	E-SAC-In	9	−40 °C - 125 °C	Paper V
D	H-SAC387	9	−40 °C - 125 °C	Paper V
D	H-SAC-In	9	−40 °C - 125 °C	Paper V
E	SAC405/FR-4	9	0 °C - 100 °C	Paper III
E	SAC405/FR-4	9	−40 °C - 125 °C	Paper III
F	SAC405/Arlon	9	0 °C - 100 °C	Paper III
F	SAC405/Arlon	9	−40 °C - 125 °C	Paper III

2.3 Non-destructive inspection

X-ray microscope Feinfocus X-ray System FXS-160.23 was used to investigate the quality of the test joints after reflow soldering and when the TCT of the test assemblies was completed.

Scanning acoustic microscopy was used to detect failures in the test modules during and/or after the TCT. C-images were produced by using the 'interface scan' technique [46]. The equipment consisted of a Sonoscan D-9000 C-mode scanning acoustic microscope and 50 MHz or 100 MHz focused transducers ($F^{\#} = 2$, pulse-echo mode). Since the scanning acoustic microscopy is not as familiar inspection technique as, for example, X-ray or SEM investigation, a short description of the method is given below.

In scanning acoustic microscopy, a transducer is excited by electrical impulses to generate ultrasonic waves (compression and shear) of a specified frequency into the material. As the ultrasound reaches the interface of dissimilar materials, a certain amount of ultrasonic energy is reflected, while the rest is transmitted through the interface. Especially, an air gap (delamination or crack) within the material causes almost complete reflection of the ultrasound wave, since the acoustic impedance of air is practically zero.

For the inspection of LTCC applications, pulse/receiver transducers over a range of 50 MHz to 230 MHz can be typically used. The selection of the transducer is based on the thickness of the laminated structure (depth penetration), the resolution requirements to be achieved (features at the layer to be investigated) and the lay-out of the application (attenuation in material and reflection coefficient for the ceramic/metallization interface).

The technique of using the same transducer to generate the initial pulse and to receive the reflected ultrasound pulses is called the pulse-echo technique. The received waveform, which is displayed as amplitude data along a time base, is called an A-scan. Scanning a sample in a raster pattern and combining all the individual A-scans, a C-scan, which is a plan-view image of a specific layer, is produced. Semmens and Kessler [46] have presented an imaging method, the 'interface scan' technique, for the characterization of flip chip interconnect failures. In the C-scan, which has been produced by the 'interface scan' technique, the dark areas indicate the sound portions of the joints, while the light contrast comes from the back-reflection of the acoustic signal due to a crack.

In Figs. 3 and 4, the SAM analysis of the LTCC/PWB assembly is demonstrated [47]. The cracking of the joints was clearly visible as light areas within the solder joint. Moreover, the blue echo related to the crack and the red echo related to the bottom of the LTCC module was overlapped in Fig. 3a. This proved that the crack existed at the interface between ceramic and metallization. In the case of ceramic cracking, a black irregular line due to material discontinuity was observed in the C scan and the blue echo related to the crack existed before the red echo related to the bottom of the LTCC module in A Scan (Fig. 3b). This showed that the crack was located within the ceramic.

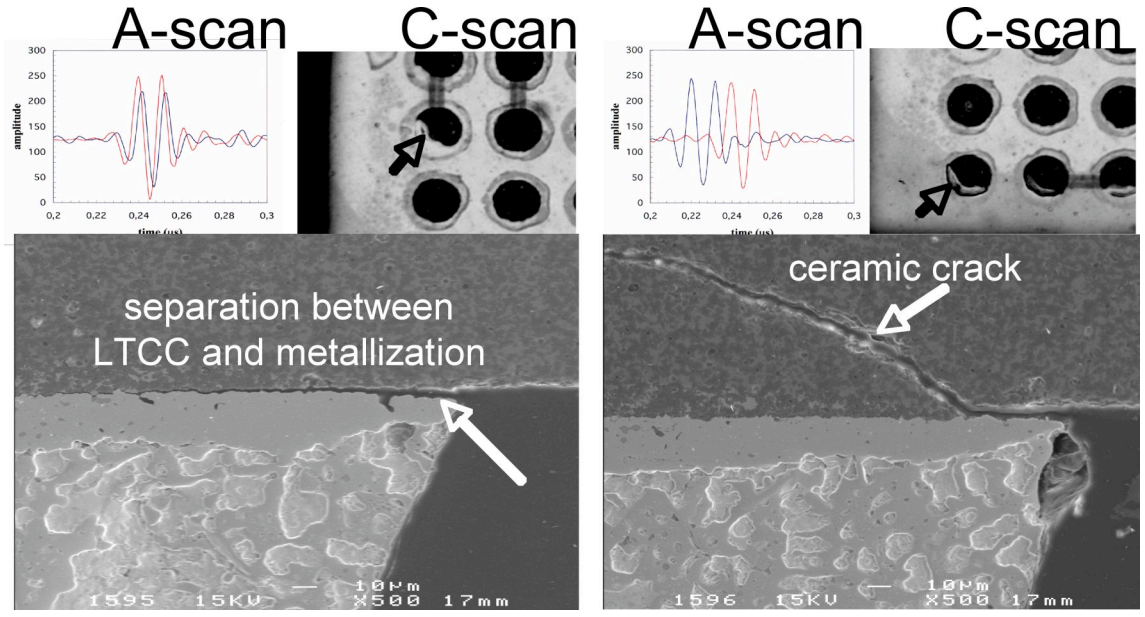

(a) **(b)**

Fig. 3. The A and C scans (230 MHz transducer, $F^{\#} = 2$) related to (a) the failures between ceramic and metallization and (b) within ceramic.

In Fig. 4, a 230 MHz transducer ($F^{\#}$ = 2) was used to ensure the separation of echoes at the layer to be investigated. The black echo related to the narrow area 1 of the joint occurred after the reference signal (red echo) on the time axis of the A-scan. This observation indicated that the crack was initiated and propagated first in the solder. The crack propagated into the ceramic afterwards, as seen from the position of blue echo, which corresponded to the area 2 of the joint in the C-scan. The black curved line between the areas 1 and 2 in the C-scan was due to a material discontinuity (crack) on the surface of the LTCC. The reference signal (red echo) in Fig. 4 was originated from the back surface of the LTCC next to the damaged joint.

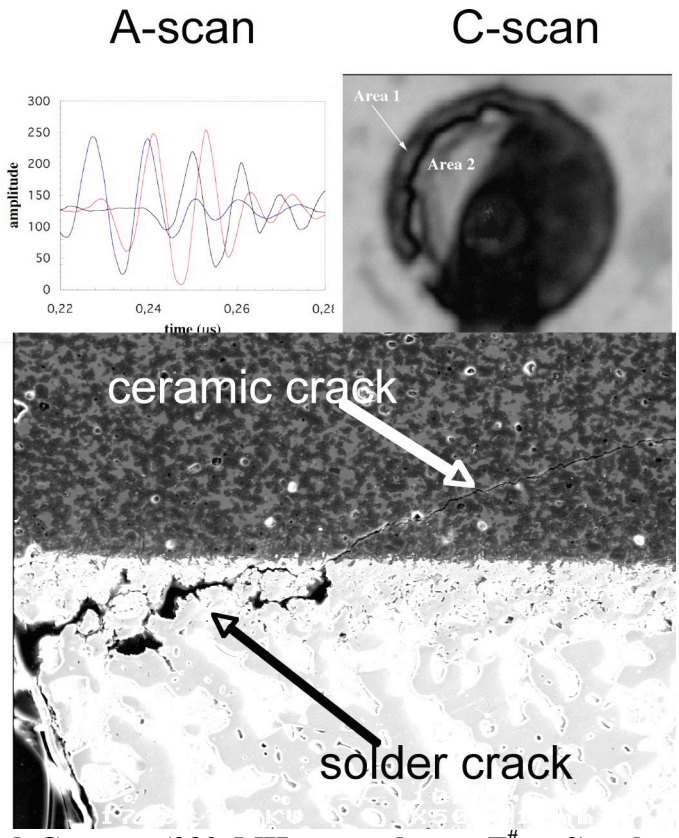

Fig. 4. The A and C scans (230 MHz transducer, $F^{\#}$ = 2) related to the failures within solder matrix and within ceramic.

As the thickness of the LTCC module is increased and the solder mask configuration is applied in the module, the use of high frequency (230 MHz) transducers is not practical. Therefore, the determination of the exact location of the crack is difficult due to the wider signal formed in the A scan procuded usin a transduces with lower frequency. The cracks within solder and cracks related to ceramic can still be easily detected since they have the different characteristic features, but the difference between the cracking at the ceramic/metallization interface and within ceramic is difficult to observe, as explained below.

The SAM analysis of the thick (1.2 mm) LTCC package is demonstrated in Fig. 5. First of all, the separate cracks formed within the solder at the inner and outer edges are easily

detected in Figs. 5a and 5b. The joints with the cracks within solder can be distinguished from the joints having a crack related to ceramic. But the black irregular line due to material discontinuity is related to the crack at ceramic/metallization interface in this case, as shown in Fig. 5d. Nevertheless, on the basis of the information of the SAM analysis, the occurrence and number of the cracks related to ceramic is known and the direction of the crack propagation can be seen comparing the location of the crack tip between the images taken during the TCT. The location of the exact crack paths can be verified afterwards using SEM.

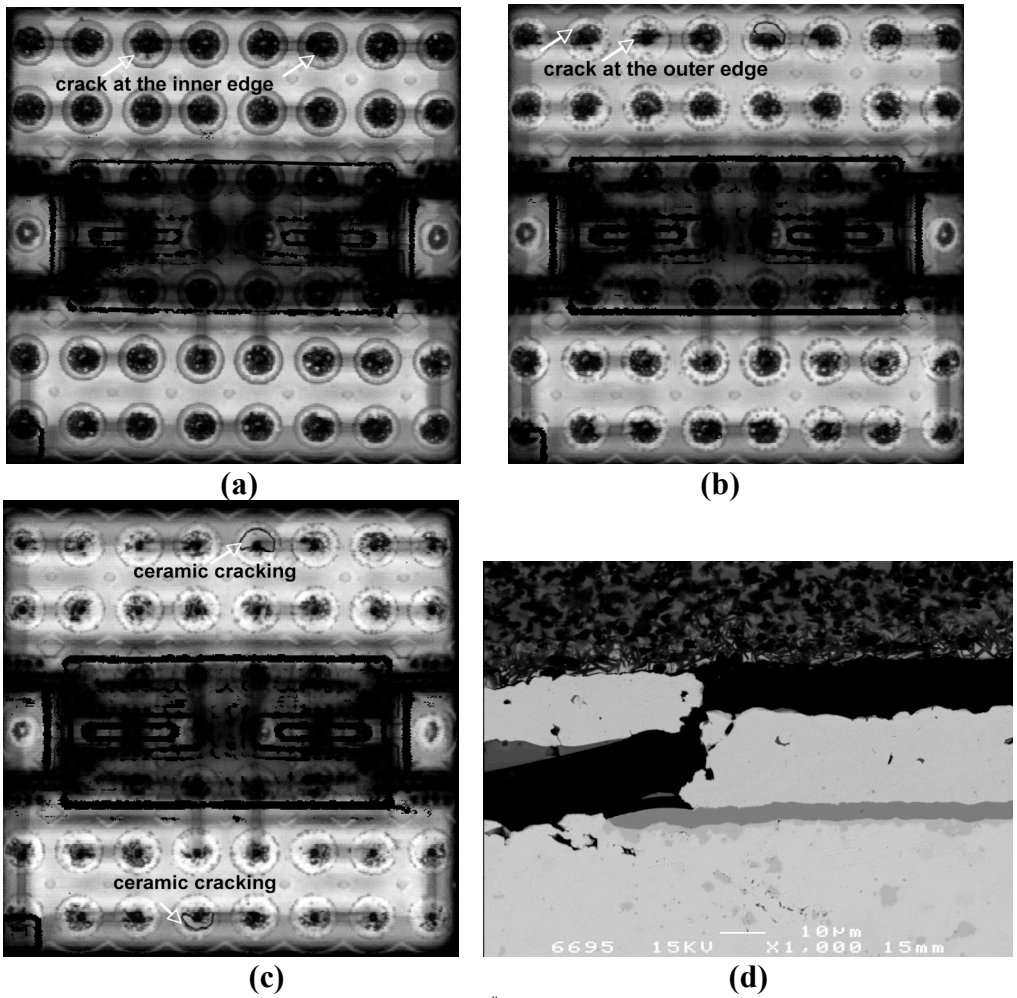

Fig. 5. The C-scans (50 MHz transducer, $F^{\#} = 2$) of the 1.2 mm thick LTCC-SiP package after (a) 100, (b) 500, and (c) 1400 cycles. (d) The origin of the black irregular line of the crack related to ceramic in Fig. 5c.

2.4 Metallography

To characterize microstructures, compositions, and crack paths within the test assemblies, SEM/EDS (Jeol JSM 6400 scanning electron microscope and INCA analyzer software)

investigations were carried out. Recrystallization of the test joints was investigated using an optical microscope with polarized light. In order to examine the fractured surfaces of the test modules using a FE-SEM (Jeol JSM-6300F), 2 - 3 modules of each test board were carefully detached from the PWBs.

3 Results

3.1 Non-destructive testing

3.1.1 X-ray investigation

A complication related to the ENIG plated test modules was observed before the 1st reflow. Cracking existed in a few ceramic solder masks of several test modules. The defected solder mask caused solder spreading along the Ag metallization. This resulted in an asymmetric solder joint geometry (Fig. 6). However, all the crucial daisy-chained joints (i.e. the joints near the corners of the module) in every test module were intact. No excessive voiding was observed in the test assemblies.

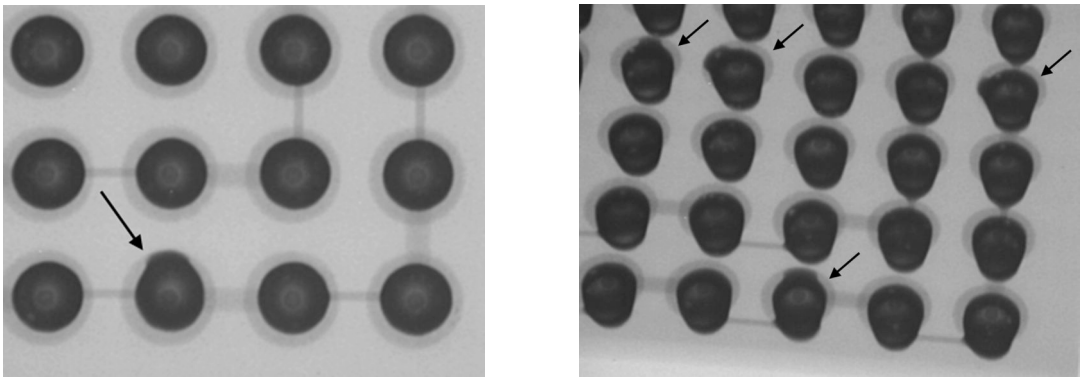

(a) **(b)**

Fig. 6. (a) A top view X-ray image of a joint with a defective solder mask and (b) an oblique view X-ray image of test joints with a few damaged solder masks.

3.1.2 Scanning acoustic microscopy

The SAM analysis of the test assemblies was performed as was presented in Chapter 2.3. The SAM analyses indicated that the separate cracks were formed in the outer and inner edges of the joint in all test assemblies similarly with the joints shown in Fig 5. The observed cracking related to the ceramic in the outer edge of the joints in the test assemblies are compiled to the Table 6.

Table 6. Ceramic cracking in the test modules after the thermal cycling tests [Papers I - V].

Assembly	test module	TCT	ceramic cracking	comments
A	SAC405	0 °C - 100°C	not detected	
A	SAC-In	0 °C - 100°C	not detected	
A	SM/FR-4	0 °C - 100°C	occasional	
A	SM/Arlon	0 °C - 100°C	not detected	
B	SAC	−40° C - 125 °C	occasional	
B	SAC-In	−40° C - 125 °C	occasional	
C	SM/FR-4	−40° C - 125 °C	primary	
C	SM/Arlon	−40° C - 125 °C	occasional	
D	E-SAC387	−40° C - 125 °C	primary	Cracks in solder mask existed before TCT
D	E-SAC-In	−40° C - 125 °C	primary	Cracks in solder mask existed before TCT
E	H-SAC387	−40° C - 125 °C	occasional	Cracks in solder mask existed before TCT
E	H-SAC-In	−40° C - 125 °C	occasional	Cracks in solder mask existed before TCT
F	SAC405	−55 °C - 150 °C	occasional	1100 μm PCSB
F	SAC-In	−55 °C - 150 °C	occasional	1100 μm PCSB

3.2 Optical microscopy with polarized light

The microstructural changes of the solder joints were investigated in Paper V. The initial microstructure of SAC-In, and SAC387 after solidification is shown in Fig. 7. In these images, a few large grains are seen in the cross-section of the soldered joint. Furthermore, recrystallization occurred in the test joints near the corners of the test modules during the TCT, as demonstrated in Fig. 8. According to the images, the initial coarse grain structure of SAC-In joints was completely turned into a recrystallized structure, whereas recrystallized areas in the other test zones were located near the ceramic/solder interface. The above-mentioned observations were made of joints near the corners of the modules, but the region between the via and the PCSB were recrystallized also in joints located in the middle of the outer row. This indicated significant inelastic deformation within this region of the present non-collapsible joint configuration.

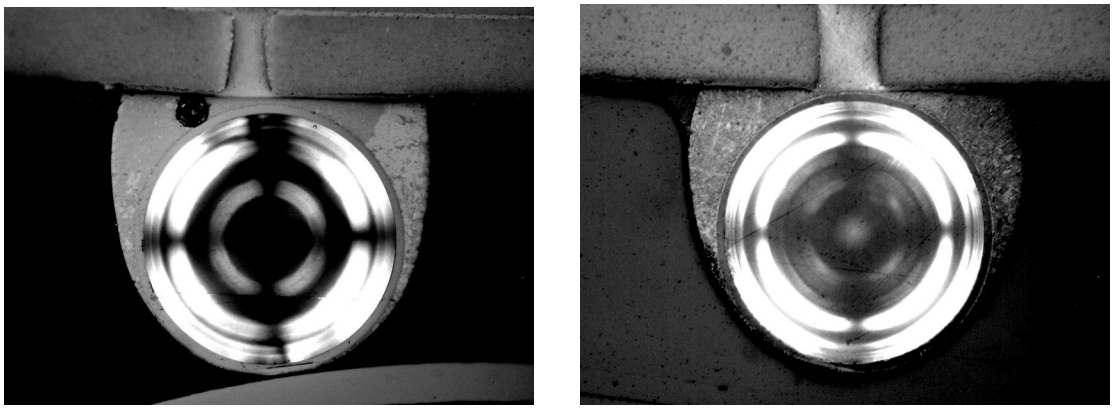

(a) **(b)**

Fig. 7. Initial microstructure of (a) SAC-In and (b) SAC387 joints [Paper V].

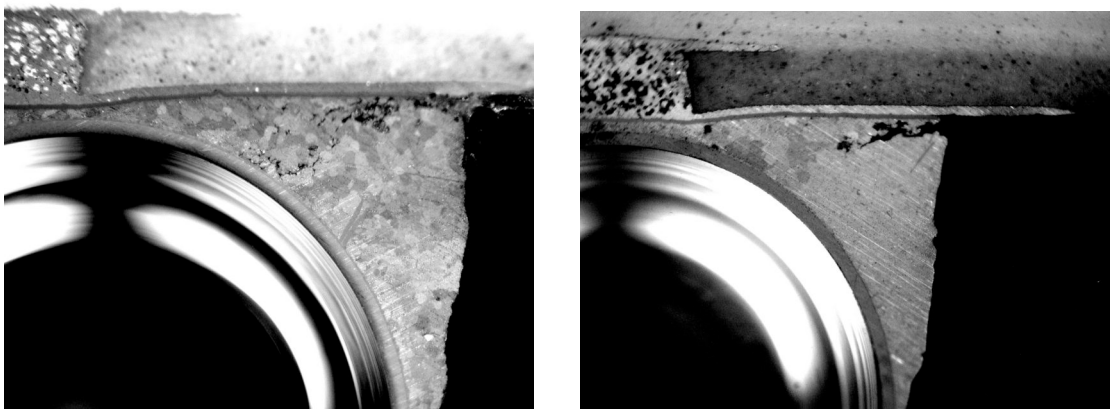

(a) **(b)**

Fig. 8. Recrystallized microstructure of (a) H-SAC-In and (b) H-SAC387 joints in test assembly D [Paper V].

It must be noted, however, that the test boards were exposed to a different number of cycles in the TCT. The test assemblies C with E-SAC387 and E-SAC-In joints were taken out of the test chamber after approximately 1100 and 1750 cycles, respectively. The test assemblies D with E-SAC387 and E-SAC-In joints were taken out of the test chamber after approximately 2000 and 2600 cycles, respectively. Thus, the amount of inelastic deformation varied in the different test joints.

3.3 SEM/EDS analyses

3.3.1 Metallurgy of the test joints

The characteristic features of the microstructure of the test solders after reflow soldering are presented in Fig 9. An intermetallic layer consisting of a $Ag_3(Sn,In)$ phase was formed between the metallization and the solder matrix of the AgPt metallized SAC-In joints (Fig 9a). The average thickness of the layer was 2 - 3 μm. The average thickness of the AgPt metallization of the test modules was approximately 11 μm. A similar layer of Ag_3Sn phase was formed in the SAC405 joints. The $Ag_3(Sn,In)$ particles within the solder matrix were globular in the SAC-In solder, whereas the thin and elongated Ag_3Sn particles are dispersed within the Sn matrix, as shown in Figs 4b and 4c. Another IMC type existing in the test solder was Cu_6Sn_5 in the ternary SAC solders and $Cu_6(Sn,In)$ in the SAC-In solder. In the SAC-In solder, a γ ($InSn_4$) phase was detected occasionally, as shown in Fig. 9b. In the ENIG plated modules, a $(Cu,Ni,Au)_6Sn_5$ layer existed in all solder lands of the test assemblies after reflow.

Furthermore, the IMC layers did not grow noticeably during the TCTs over temprature ranges 0 °C - 100 °C and –40 °C - 125 °C. The interface between them and the solder matrix was practically free from Kirkendall voids after the TCT. However, the composition of the IMC layer changed to $(Cu,Ni,Au)_6(Sn,In)_5$ in the ENIG plated SAC-In joints during the TCT, but the atomic fraction of indium was small (1 - 3%) in this layer.

The indium content in $Ag_3(Sn,In)$ and $Cu_6(Sn,In)_5$ particles within the solder matrix was also slightly increased. In the case of the ternary SAC solders, only slight coarsening of the IMC particles was observed after the TCT. Finally, phosphorous-rich particles were occasionally detected within the IMC layer after the first reflow. These particles did not grow during the TCT, but their size remained at less than a micron.

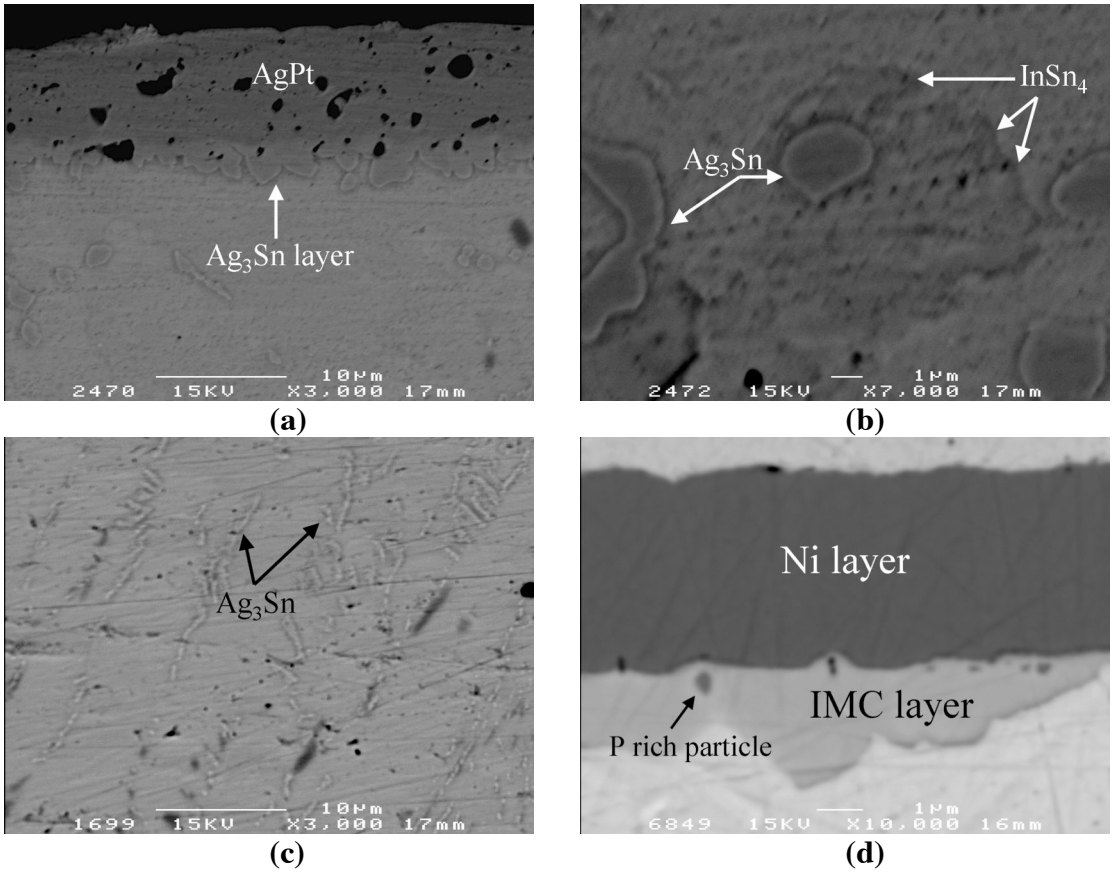

Fig. 9. The characteristic features of the as-solderd test joints: (a) an IMC layer and (b) $InSn_4$ phases (white arrows) in the AgPt metallized SAC-In joint. (c) Dispersed IMC particles in a ternary SnAgCu alloy. (d) The IMC layer of an ENIG plated test joint [Papers IV and V].

The EDS analysis of the as-soldered microstructure of the SAC-In joints is given in Table 7. It must be noted that the amount of tin in the γ ($InSn_4$) phase is an overestimation, since the width of the phase is less than 0.5 µm (Fig. 9b) and the spatial resolution of EDS analysis is typically over 1 µm.

Table 7. Average and standard deviation of elements in the SAC-In solder after the first reflow soldering [Paper IV].

Phase	Sn (at%)	In (at%)	Ag (at%)	Cu (at%)
Sn matrix	96.65±0.98	3.35±1.24	n.d.	n.d.
γ ($InSn_4$)	88.01±0.98	11.99±1.29	n.d.	n.d.
$Ag_3(Sn,In)$	18.24±3.04	7.07±3.07	74.69±1.27	n.d.
$Cu_6(Sn,In)_5$	45.75±1.63	2.95±1.07	n.d.	51.30±1.79

n.d. = not detected

The EDS analysis of the microstructure of the SAC-In joints after the TCT over a temperature range of –55 °C - 150 °C is given in Table 8. Firstly, it must be noted that the indium content of the Sn matrix was under the reliable detection limit of the EDS analysis. Furthermore, no γ ($InSn_4$) phase could be detected anymore in the joints. Another interesting point is homogenization of the indium content in the slightly coarsened globular $Ag_3(Sn,In)$ particles.

Table 8. Average and standard deviation of elements (in the IMCs of SAC-In solder after the TCT over a temperature range of –55 - 150°C [Paper IV].

IMC	Sn (at%)	Ag (at%)	Cu (at%)	Ni (at%)	In (at%)	Au (at%)
$Ag_3(Sn,In)$	19.30±1.33	74.93±1.10	n.d.	n.d.	5.77±1.83	n.d.
$Cu_6(Sn,In)_5$	45.05±1.22	n.d.	52.94±0.31	n.d.	2.01±0.08	n.d.

n.d. = not detected

3.3.2 Crack paths of collapsible SAC405 joints

In the case of the test assemblies E tested under the harsh test condition (–40 °C - 125 °C), ceramic cracking typically occurred, as shown in Fig. 10a. Occasionally, the failure was located completely within the solder joint. In that case, the crack formed in the inner edge of the joint was located between the Ag_3Sn layer and the Sn solder matrix, whereas the crack formed in the outer edge of the joint propagated within the solder matrix. Moreover, the crack that formed between the Ag_3Sn layer and the solder in the inner edge of the joint was a typical feature of all the test assemblies. In the case of the LTCC/Arlon assemblies the both crack paths were located within the solder (Fig. 10b).

Considering the failure at the outer edge of the joints, severe intergranular cracking could often be observed in the region at the outer edge of the collapsible joint after the TCT over a temperature range of 0 °C - 100°C. This indicated that intergranular creep cracking was the dominant failure mechanism of the crack formed at the low temperature extreme in both assemblies tested over a temperature range of 0 °C - 100°C. The detected cracks that formed in the joints of the test assembly F at the low temperature extreme of the harsh test, propagated within the solder matrix, but their exact failure mode could not be determined.

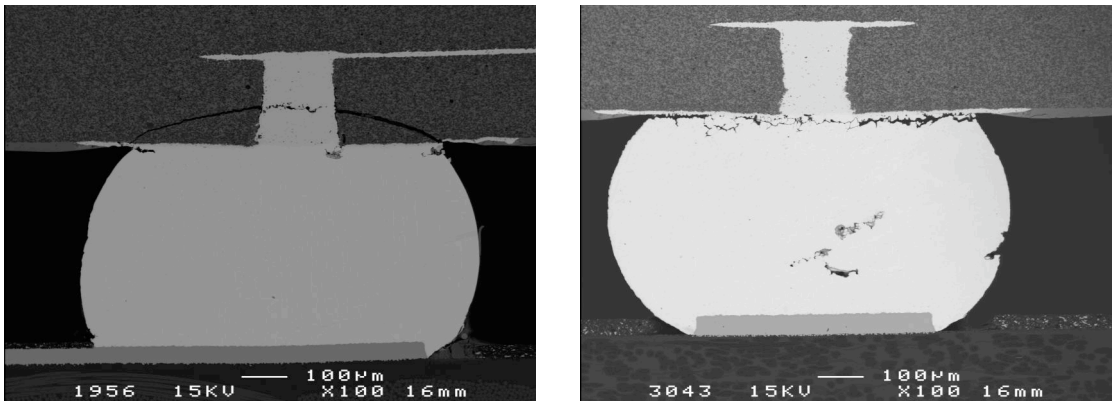

(a) **(b)**

Fig. 10. Characteristic crack paths in the collapsible joints of the test assembly E after the TCT over a temperature range of –40 °C - 125 °C. (b) Characteristic crack paths in the collapsible joints of the test assemblies E and after the TCT over a temperature range of 0 - 100°C and the test assembly F the TCT over a temperature range of –40 °C - 125 °C [Paper III].

The summary of the crack paths observed in the collapsible test joints is given in Table 9.

Table 9. Location of the primary crack paths after the thermal cycling tests [Paper III].

Joint type	TCT	Outer edge	Inner edge
SAC405/FR-4	0 °C - 100°C	within solder matrix	at IMC/solder interface + within solder matrix
SAC405/Arlon	0 °C - 100°C	within solder matrix	at IMC/solder interface + within solder matrix
SAC405/FR-4	–40° C - 125 °C	in ceramic	at IMC/solder interface + within solder matrix
SAC405/Arlon	–40° C - 125 °C	within solder matrix	at IMC/solder interface + within solder matrix

3.3.3 Crack paths of non-collapsible SAC405 and SAC387joints

The SAM investigation indicated that separate cracks existed at the outer and the inner edge of the joints and they propagated towards the center area of the ternary SAC405 joints. These two cracks of the joints tested in the temperature range of 0° C – 100 °C are shown in Fig. 11a. A few different features can be observed from the cross-sectional specimens compared with the joints tested in the temperature range of –40° C – 125 °C (Fig. 11b). Firstly, the crack that propagated away from the neutral point was not located strictly at the IMC/solder interface, but more solder cracking was observed. Finally, there were more secondary cracks on the PWB side of the joint. These observations indicate that the milder test conditions have changed the creep/fatigue behavior of the test joints. The crack paths were located similarly in the SAC405 joints tested in the temperature range of –55° C – 150 °C, except that severe intergranular cracking often occurred on the inner side of these joints, as shown in Fig. 11c.

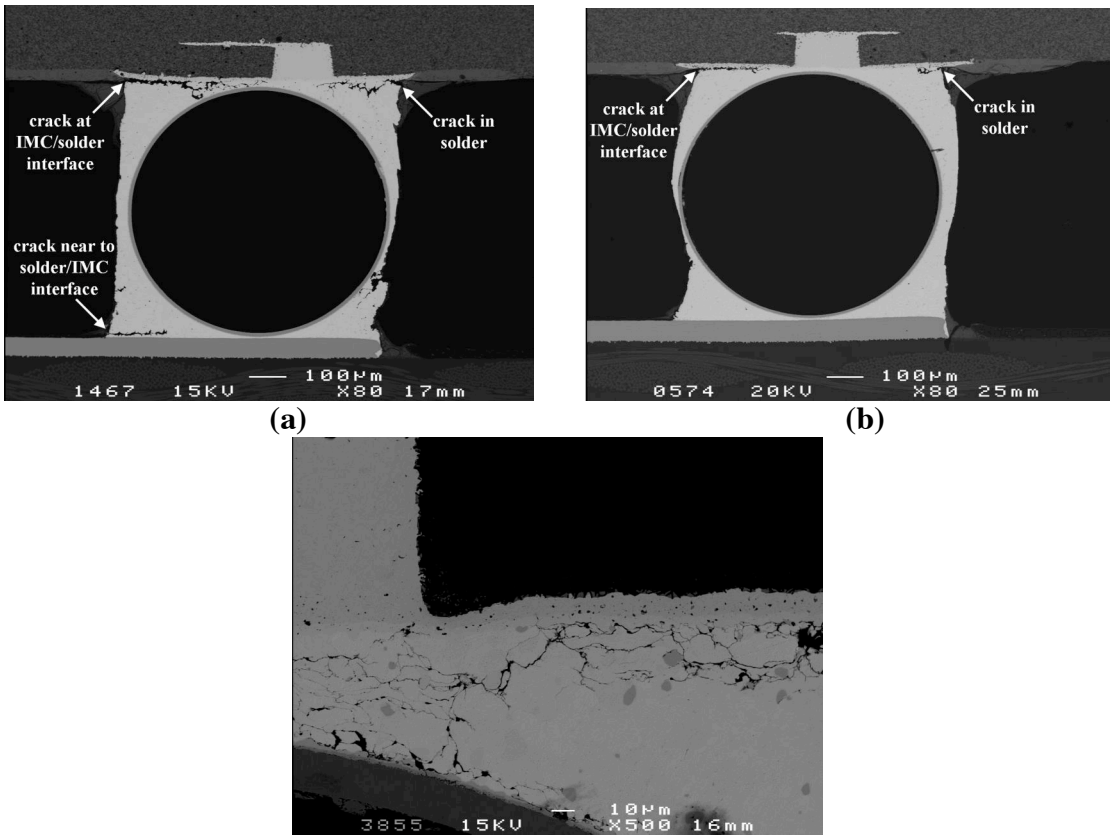

Fig. 11. Characteristic crack paths of the SAC405 joints of the test assemblies A and B after the thermal cycling test over temperature ranges of 0 - 100°C, (b) –40 °C - 125 °C. (c) Severe intergranular cracking on the inner side of the SAC405 joint after the TCT over temperature range –55 °C - 150 °C [Papers I and IV].

The characteristic crack paths in the solder matrix of the SAC387 joints on the LTCC side after the TCT are shown in Fig. 12. Cracking within solder detected in these joints were comparable with the primary failure of the test joints of assembly A (see Fig. 11b). Furthermore, the SEM analysis revealed that a separate intergranular fracture could form in the middle of the joint during the TCT, as shown in Fig. 12b. However, the SAM analysis indicated that the joints of the assembly C suffered primarily from cracking at ceramic/metallization interface (see Table 6).

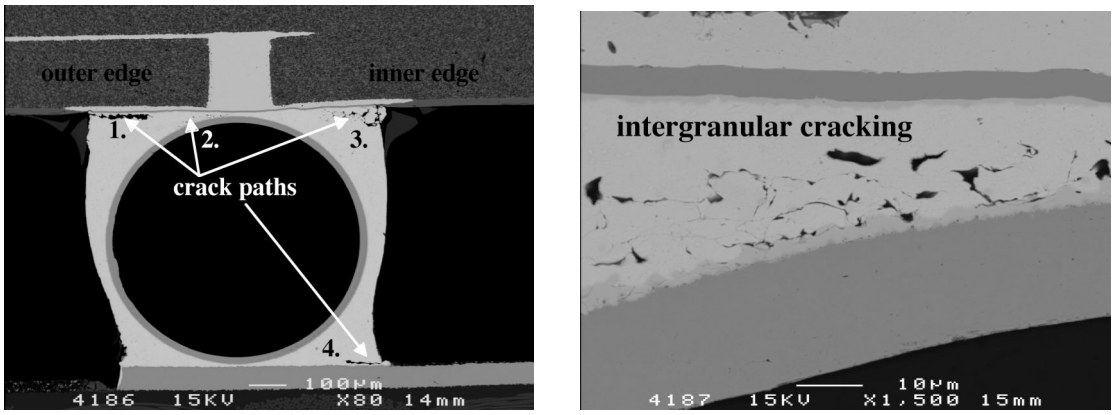

(a) **(b)**

Fig. 12. Characteristic crack paths of the SAC387 joints of the test assembly C and D and (b) an enlarged image of the 2nd crack path after the thermal cycling test over temperature range –40 °C - 125 °C [Paper V].

3.3.4 Crack paths of non-collapsible SAC-In joint configurations

In the case of the SAC-In joints of the test assemblies A, C and D, the SEM investigations of the cross-sectional samples proved that the cracks formed in the inner and outer edges of the joint propagated characteristically in the solder matrix after the TCTs over temperature ranges 0 °C - 100 °C and –40 °C - 125 °C, as demonstrated in Figs. 13a and 13b. Severe intergranular cracking could often be observed in the region of the inner edge of a joint. These observations indicated that intergranular creep cracking was the dominant failure mechanism of cracks formed at the high temperature extreme. Moreover, the rugged crack path of the failure formed at the low temperature extreme suggested that a similar failure type existed at the outer edge of the joints. When this joint type was exposed to the extremely harsh TCT over a temperature range –55 °C - 150 °C, the crack path was located at the $Ag_3(Sn,In)$/solder interface at the inner edge of the joint, whereas the crack formed at the outer edge propagated within the solder matrix (Fig.13c). The thickness of the $Ag_3(Sn,In)$ layer varied from 5 - 7 µm after the TCT.

The characteristic crack paths of the ENIG plated SAC-In joints are shown in Fig. 13d. Cracking in the mixed ceramic/metallization zone was the primary failure mechanism in the joints of assembly C, whereas the occasional failures within solder detected in these joints were comparable with the primary failure of the test joints of assembly D (Fig. 13d). Furthermore, the SEM analysis revealed that a separate intergranular fracture could form in the middle of the joint during the TCT.

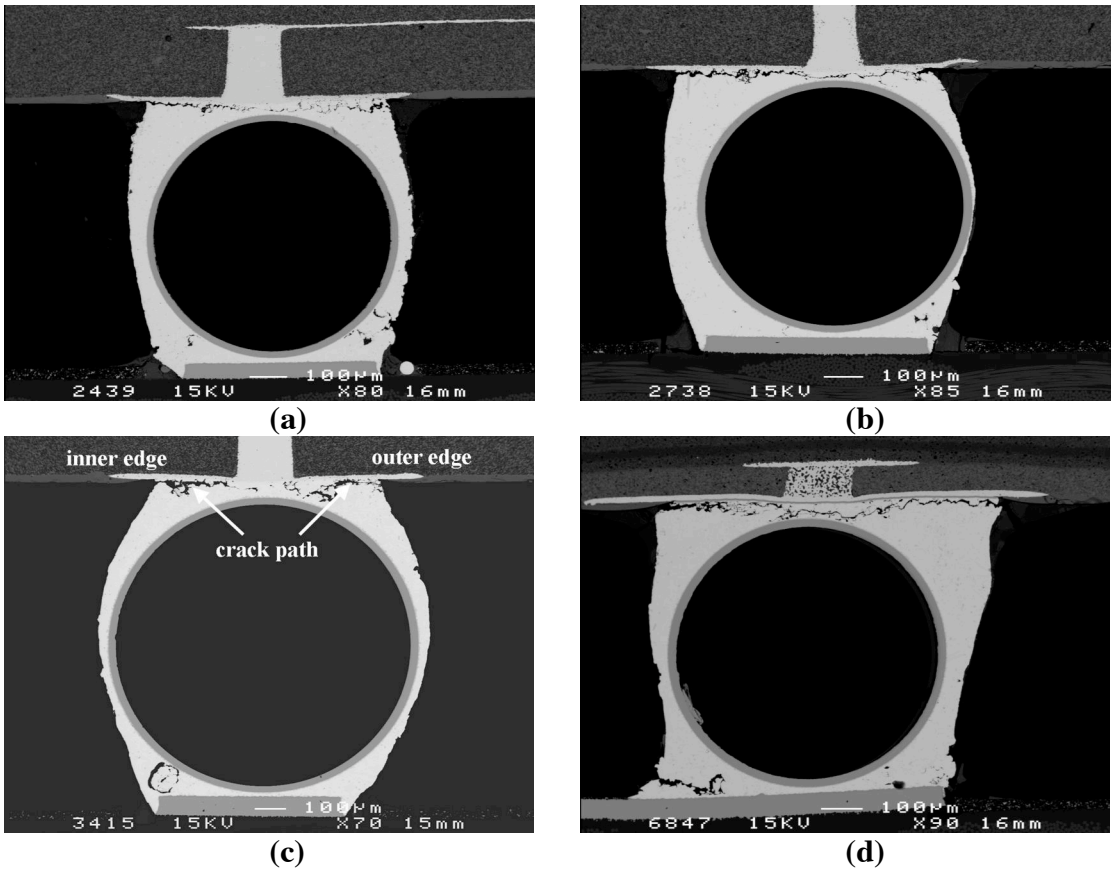

Fig. 13. Characteristic crack paths of the AgPt metallized SAC-In joints after the thermal cycling test over temperature ranges of 0 - 100°C, (b) –40 °C - 125 °C, and –55 °C - 150 °C. (d) Characteristic crack paths of the ENIG plated SAC-In joints after the thermal cycling test over a temperature range of –40 °C - 125 °C [Papers II, IV and V].

The summary of the crack paths observed in the non-collapsible test joints is given in Table 10.

Table 10. Location of the primary crack paths after the thermal cycling tests [Papers I,II, IV and V].

Joint type	TCT	Outer edge	Inner edge	comments
SAC405	0 °C - 100°C	within solder matrix	at IMC/solder interface + within solder matrix	
SAC-In	0 °C - 100°C	within solder matrix	within solder matrix	
SAC405	−40° C - 125 °C	within solder matrix	at IMC/solder interface	
SAC-In	−40° C - 125 °C	within solder matrix	within solder matrix	
E-SAC387	−40° C - 125 °C	at ceramic/metallization interface	within solder matrix	*within solder matrix in some critical joints
E-SAC-In	−40° C - 125 °C	at ceramic/metallization interface	within solder matrix	*within solder matrix in some critical joints
H-SAC387	−40° C - 125 °C	within solder matrix	within solder matrix	
H-SAC-In	−40° C - 125 °C	within solder matrix	within solder matrix	
SAC387	−55 °C - 150 °C	within solder matrix	at IMC/solder interface	
SAC-In	−55 °C - 150 °C	within solder matrix	at IMC/solder interface + within solder matrix	

3.4 FE-SEM analyses

3.4.1 Failure mechanisms of the collapsible SAC405 joints

The main characteristic features of the fracture surface of the joints in the test assemblies E and F after the thermal cycling tested over a temperature range of –40 °C - 125 °C are presented in Figs. 14 and 15. In the case of the F assembly, tin grains with damaged grain boundaries were typically observed on the fracture surface of at outer edge of the joint, as shown in Fig. 14b. This proved the creep-related nature of the failure. On the other hand, the main characteristic features of the outer fracture surface of a joint in the assembly E differed from the above-mentioned failure. A narrow zone where the grain size is smaller compared with the inner area of the fracture surface was seen at the outer edge of the joint surface (Fig. 15b). The characteristic feature of this region was the existence of fatigue striations, proving that the thermally induced failure propagated in a transgranular manner (Fig. 15c).

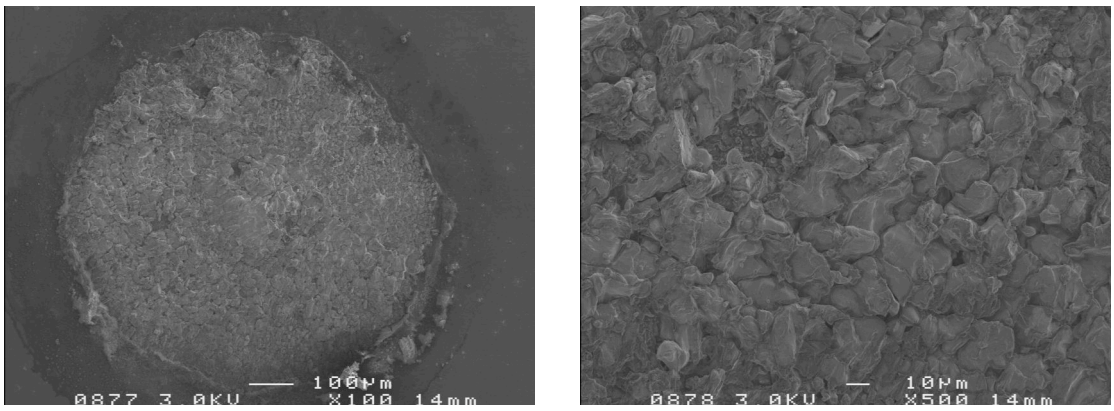

(a) **(b)**

Fig. 14. Fracture surfaces on the LTCC side of a collapsible SAC405 joint of the assembly after F the thermal cycling test over the temperature range of –40 °C - 125 °C: (a) the whole area, and (b) the fractured surface at the outer edge [Paper III].

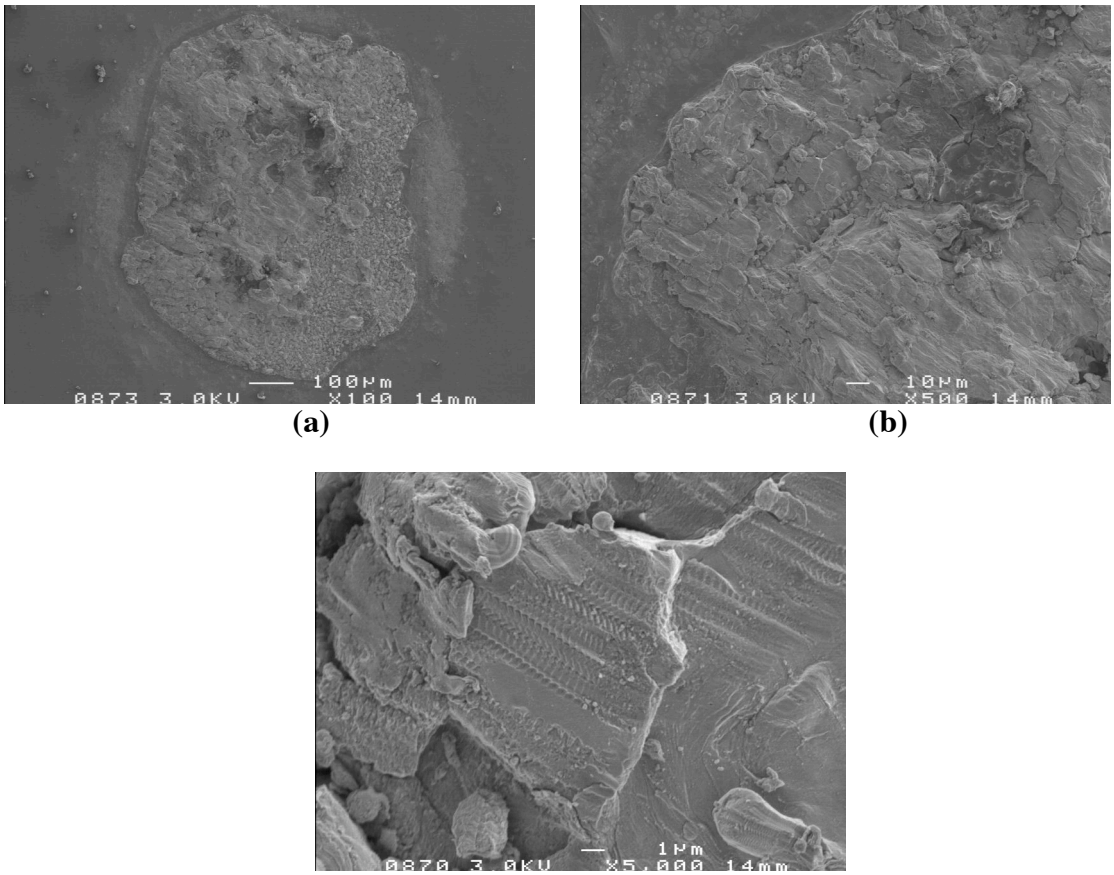

(a) **(b)**

(c)

Fig. 15. Fracture surfaces on the LTCC side of a collapsible SAC405 joint of the assembly E after the thermal cycling test over the temperature range of –40 °C - 125 °C: (a) the whole area (b) the fractured surface at the outer edge, and (c) indication of transgranular fatigue cracking within the narrow zone of Fig. 12 b. [Paper III].

The summary of the primary failure mechanisms observed in the collapsible test joints is given in Table 11.

Table 11. Primary failure mechanisms of the collapsible test joints after the TCT over temperature ranges of 0 °C - 100 °C and –40 °C - 125 °C [Paper III].

assembly	TCT	ceramic cracking	mixed transgranular/intergranular	intergranular	failure at IMC/solder interface
E	0 °C - 100 °C	n.d.	n.d.	outer edge	inner edge
F	0 °C - 100 °C	n.d.	n.d.	outer edge	inner edge
E	–40 °C - 125 °C	outer edge	(outer edge)	n.d.	inner edge
F	–40 °C - 125 °C	n.d.	n.d.	outer edge	inner edge

n.d. = not detected
(location) = occasional observations

3.4.2 Failure mechanisms of the non-collapsible joints

In an LTCC module with BGA joints, the critical joints (i.e. joints with the highest stress level) are typically located in the corners of the module. A typical fracture surface on the LTCC side of the SAC405 corner joint of the test assembly A after the TCT over a temperature range of 0 °C - 100 °C is presented in Fig. 16a. An intergranular fracture surface located at the outer edge of the joint is shown in Fig. 16b. In this case, neither transgranular fatigue nor the formation of the zone with fine (≈ 5 - 10 μm) grain size was detected. The surface of the inner edge consisted of less Ag_3Sn particles and more tin compared with the fracture surface formed in the harsh TCT, as shown in Fig. 16c.

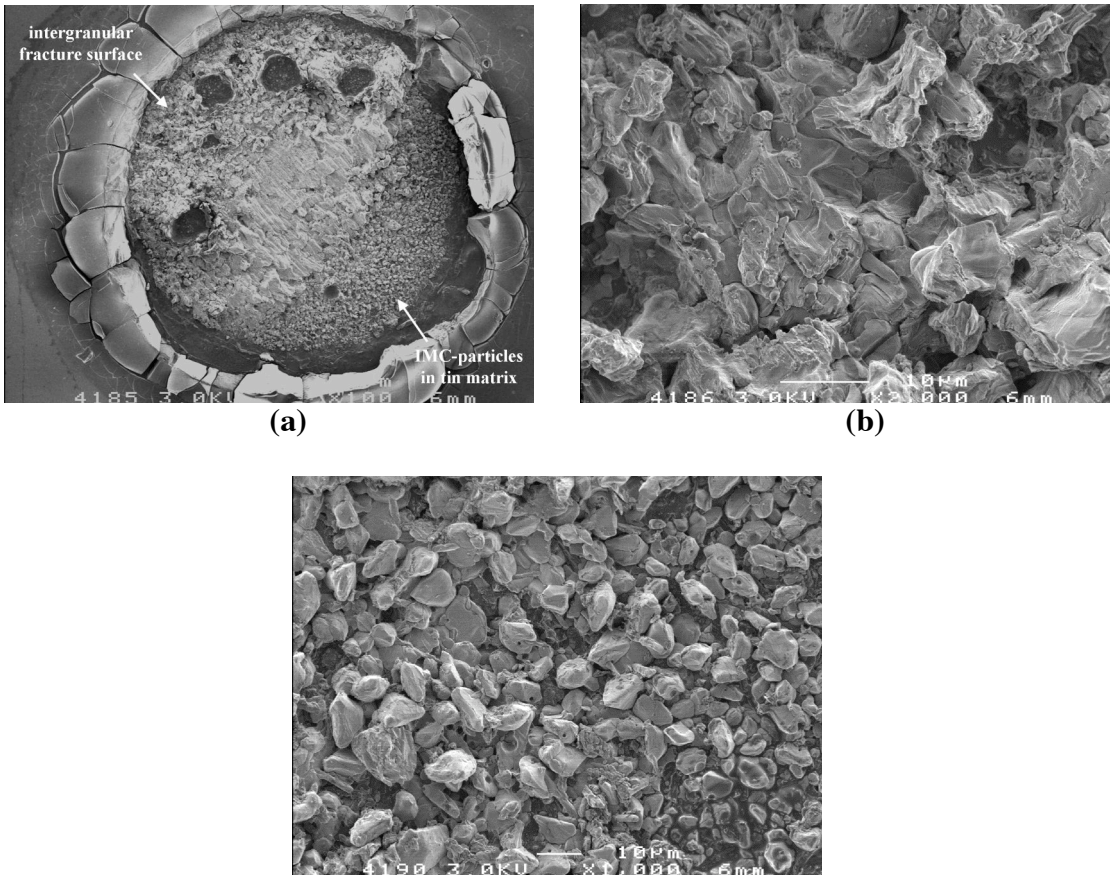

(a) **(b)**

(c)

Fig. 16. Different fracture surfaces on the LTCC side of a SAC405 corner joint after the thermal cycling test over the temperature range 0 °C - 100 °C: (a) the whole area (magnification x 100) (b) the area of the outer edge, and (c) the area of the inner edge [Paper I].

In the case of the TCT over a temperature range of –40 °C - 125 °C, the inner edge contained mainlyAg_3Sn particles. The main characteristic features of the outer fracture surface are presented in Figs. 17a-c. An 80 μm wide zone, where the grain size is smaller (≈ 5 - 10 μm) compared with the inner area of the fracture surface, is seen at the outer edge of the joint surface (Fig. 17b). This observation suggests that localized recrystallization

occurred in the critical area of the joint (i.e. the location of the highest stress/strain) during thermal cycling. Furthermore, there were several intergranular cracks on the fracture surface, indicating severe creep-related damage. Another characteristic feature was the existence of fatigue striations, proving that the thermally induced failure also propagated in a transgranular manner due to thermal fatigue, as shown in Fig. 17b. Next to the recrystallized zone was an approximately 200 - 300 μm wide zone with a coarser (≈ 10 - 20 μm) microstructure (enlarged in Fig. 17c).

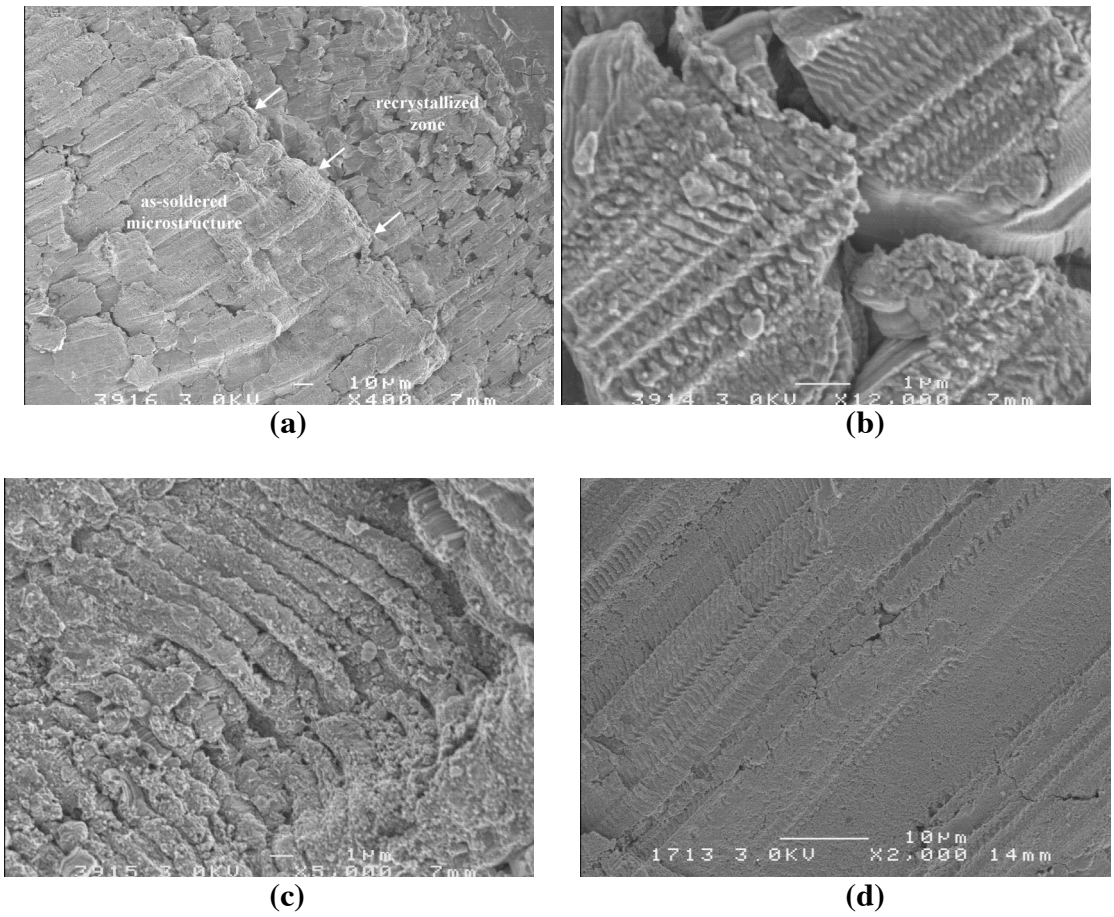

(a) **(b)**

(c) **(d)**

Fig. 17. Fracture surfaces on the LTCC side of a joint formed at (a) the low temperature extreme during the thermal cycling test over a temperature range of –40 °C - 125 °C, (b) an enlarged image of a zone with coarse grain size, and (c) an enlarged image of zone with coarse grain size. (d) Transgranular failure at the outer edge of the SAC405 joint after the thermal cycling test over a temperature range of –55 °C - 150 °C White arrows show the site of a transition from the zone with fine grain size to area of the coarse grainsin Fig. 17a [Paper I].

A fracture surface of an SAC387 corner joint of assembly B after the TCT is shown in Fig. 18a. A mixed intergranular/transgranular fracture surface was detected within the solder matrix at the outer edge of the joint (Fig. 18b), whereas the surface of the inner edge was formed by a transgranular mechanism (creep). Furthermore, a large creep failure exists in the middle of the joint. This is related to notable inelastic deformation and

subsequent recrystallization observed using SEM and the optical microscopy with polarized light (see Figs. 8b and 12b). The fracture surface consisted of a Sn-based solder matrix, although small areas of $(Cu,Ni,Au)_6Sn_5$ phase were detected near the inner edge in some joints.

Enlarged images of the outer edges of both assemblies A and B are shown in Figs. 18c and 18d. These failures revealed transgranular features with striations; the average width of a striation was approximately 0.5 μm and 0.1 μm in the joints of assembly C and D, respectively. Figs. 18b - 18d show that both transgranular cracking due to fatigue and intergranular cracking due to creep formed at the low temperature extreme.

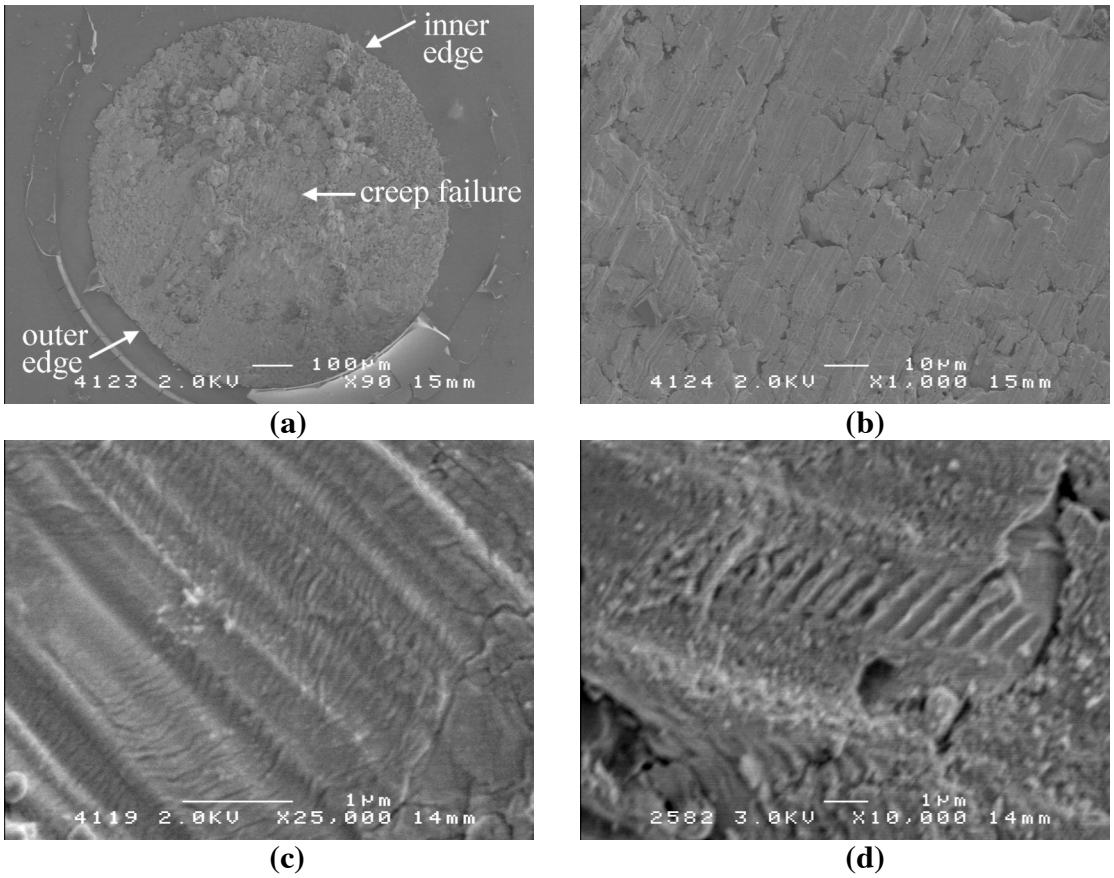

Fig. 18. Fracture surfaces on the LTCC side of E-SAC387 joints formed at the low temperature extreme during the thermal cycling test over a temperature range of –40 °C - 125 °C. (a) The fracture surface of the joint of the test assembly D, (b) transgranular failure at the outer edge of the joint and (c) an enlarged image of the outer edge of the joint. (d) Striations on the fracture surface of a E-SAC387 joint in the test assembly C [Paper V].

The typical features of the fracture surface of a SAC-In composite joint after the thermal cycling test over a temperature range of –40 °C - 125 °C are presented in Figs. 19a - 19d. Three regions can be observed on the fracture surface shown in Fig. 19a. These are the regions of intergranular creep cracking at the inner edge of the joint (enlarged in Fig. 19b) and at the outer edge of the joint (enlarged in Fig. 19c). The region in the middle of

the surface is related to either a rapid failure due to overloading that occurred after the thermal fatigue cracks reached a critical length, or a failure that occurred during the detachment of a module. Occasionally, striations can be observed on the surface of a few Sn grains, as shown in Fig. 19d.

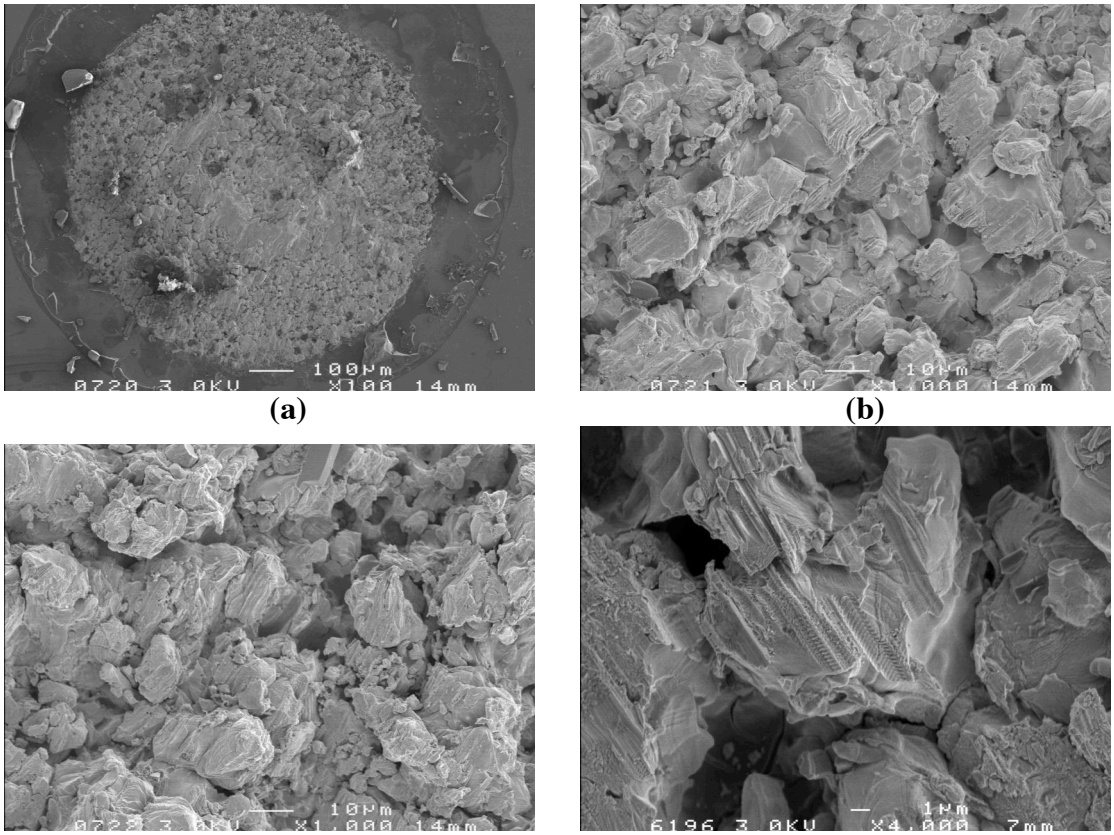

Fig. 19. Typical fracture surfaces on the LTCC side of a SAC-In corner joint after the thermal cycling test over the temperature range –40 °C - 125 °C: (a) the whole area (magnification x 100) (b) the area at the outer edge, (c) the area at the inner edge, and (d) occasional indication of transgranular fatigue cracking [Paper II].

A fracture surface of an SAC-In corner joint after the TCT over a temperature range of –55 °C - 150 °C is presented in Fig. 20a. A transgranular fracture surface within the solder matrix is seen at the outer edge of the joint, whereas the surface of the inner edge consists of homogenous $Ag_3(Sn,In)$ particles. In the case of the SAC405 joints, the fractured area consisting of Ag_3Sn particles was larger in these joints compared with the SAC-In joints. Furthermore, a large creep failure exists in the middle of the joint.

Enlarged images of the outer edge of the both test joints are shown in Figs. 20b and 20c. The failures have primarily transgranular features with striations. Occasional cracks can be detected along the boundaries of Sn grains, especially near the outer edge of the joint. These observations indicated that both transgranular cracking due to fatigue and minor intergranular cracking due to creep formed at the low temperature extreme. Finally, the

average width of a striation can be estimated from Figs. 20b and 20c, being approximately 0.6 μm and 1.2 μm in the SAC-In and SAC405 joints, respectively.

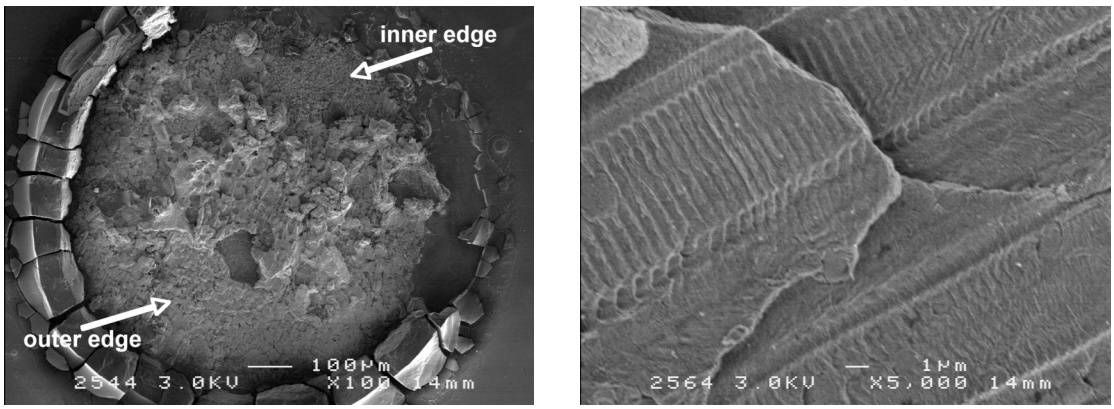

(a) **(b)**

Fig. 20. Typical fracture surfaces on the LTCC side of a SAC-In corner joint after the thermal cycling test over the temperature range –55 °C - 150 °C: (a) The fracture surface of the SAC-In joint and (b) transgranular failure at the outer edge of the SAC-In joint [Paper IV].

The summary of the primary failure mechanisms observed in the non-collapsible test joints is given in Table 12.

Table 12. Primary failure mechanisms within the non-collapsible test joints after the TCTs over temperature range of 0 °C - 100 °C, –40 °C - 125 °C, and –55 °C - 150 °C [Papers I, II, IV and V].

Temperature range of 0 °C - 100 °C		
Joint type	*Outer edge*	*Inner edge*
SAC405		Separation between Ag_3Sn layer and solder matrix
SAC-In	Intergranular (creep) cracking within solder matrix	Intergranular (creep) cracking within solder matrix
Temperature range of −40 °C - 125		
Joint type	*Outer edge*	*Inner edge*
SAC405	Mixed intergranular cracking (creep) and trasnsgranular cracking (fatigue) failure within solder matrix	Separation between Ag_3Sn layer and solder matrix
SAC-In	Intergranular (creep) cracking within solder matrix	Intergranular (creep) cracking within solder matrix
E-SAC387	Mixed intergranular cracking (creep) and trasnsgranular cracking (fatigue) failure within solder matrix	Intergranular (creep) within solder matrix
E-SAC-In	Intergranular (creep) cracking within solder matrix	Intergranular (creep) cracking within solder matrix
H-SAC387	Mixed intergranular cracking (creep) and trasnsgranular cracking (fatigue) failure within solder matrix	Intergranular (creep) cracking within solder matrix
H-SAC-In	Intergranular (creep) cracking within solder matrix	Intergranular (creep) cracking within solder matrix
Temperature range of −55 °C - 150		
SAC387	Mixed intergranular cracking (creep) and trasnsgranular cracking (fatigue) failure within solder matrix	
SAC-In	Mixed intergranular cracking (creep) and trasnsgranular cracking (fatigue) failure within	

solder matrix

3.5 Thermal cycling tests

After the thermal cycling test, the cumulative failure distribution of the test versions was determined using "Weibull ++" software. The characteristic lifetime (θ) of the joints and the Weibull shape parameter (β) are listed in Table 11.

Table 13 Characteristic lifetime θ and Weibull shape factor β values of the collapsible and non-collapsible test joints in the TCTs over temperature ranges of 0 °C - 100 °C, –40 °C - 125 °C and –55 °C - 150 °C [Papers I - V].

Assembly	Joint configuration	TCT	θ	β
A	SAC405	0 °C - 100 °C	4298 cycles	5.4
A	SAC-In	0 °C - 100 °C	5590 cycles	6.3
D	SAC405/FR-4	0 °C - 100 °C	1475 cycles	9.1
D	SAC405/Arlon	0 °C - 100 °C	5424 cycles	11.8
A	SAC405	-40 °C - 125 °C	917 cycles	6.8
A	SAC-In	-40 °C - 125 °C	1432 cycles	5.3
D	SAC405/FR-4*	-40 °C - 125 °C	524 cycles	5.6
D	SAC405/Arlon	-40 °C - 125 °C	1575 cycles	29.7
A	E-SAC387*	-40 °C - 125 °C	957 cycles	7.1
A	E-SAC-In*	-40 °C - 125 °C	1371 cycles	6.2
A	E-SAC-InNi *	-40 °C - 125 °C	1368 cycles	8.1
C	H-SAC387	-40 °C - 125 °C	1835 cycles	10.1
C	H-SAC-In	-40 °C - 125 °C	2325 cycles	9.0
B	SAC387**	-55 °C - 150 °C	531 cycles	1.3
B	SAC-In**	-55 °C - 150 °C	941 cycles	4.5

* primary failure mechanism: ceramic cracking

** 1100 μm PCSB

4 Discussion

4.1 Microstructure of solder joints

The initial microstructure of the test joints was determined after the ball attachment process (i.e. the first reflow). It must be noted that the nominal composition of upper half of the non-collapsible solder joint will evidently change in some extent during the second reflow soldering. This is due to the copper dissolution from the PCSB to the liquid solder and the mixing of the different solders used in the non-collapsible test joints. Furthermore, solid/liquid interactions between metallized pad and liquid will probably cause variation in the composition of the solder matrix near the solder/metallization interface. Finally, the test joints were fabricated using commercial solder pastes. Therefore, slight variations in their composition may exist compared with the nominal compositions given by the manufacturers due to the impurities and the fabrication process of the solder pastes.

4.1.1 SAC joints

The as-soldered joints with the SAC387 and SAC405 solders consisted of large Sn grains where Ag_3Sn and Cu_6Sn_5 particles were embedded, as shown in Figs. 7b and 9c. This is in consistence with the several studies focused on the microstructural features of BGA joints with SAC solders [48-59], although it was also reported that a large number of randomly orientated equiaxial grains were formed in small (300 μm) SAC solder balls cast in a alumina mould [57,58]. The Ag content of the alloy had the main effect on the characteristic features of the solidified microstructure in the practical reflow conditions of the common commercial SAC solder pastes [48,53,60]. On the other hand, the Cu content of these pastes varies typically from 0.5 wt% to 0.7 wt%. Thus, its effect on the variation of the solidified microstructure is lesser compared with the 1 - 4 wt% Ag content of the solders. Since the nominal Ag content of the ternary SAC solder alloys used in this work were 3.8 wt% and 4 wt% and the reflow conditions were practically similar, there was no significant difference between the initial microstructure of the test joint.

The initial microstructure will evidently change during the TCT test. Dutta et al. [61] reported substantial strain-induced and static coarsening of Ag_3Sn particles within small (100 μm) Sn4Ag0.5Cu BGA solder joints exposed to the extremely severe TCT over a temperature range –65 °C - 160 °C. Similar behaviour was observed in the solder joints of the ceramic chip resistors tested over a temperature range –40 °C - 125 °C [62]. However, no significant coarsening of the IMC particles within the solder matrix of the test joints was detected after the TCT [Papers I and III]. This was due to the fact that the strain was mainly localized in the narrow recrystallized zone of the test joint configurations. Thereby, it can concluded that the moderate coarsening of the IMC particles within the bulk solder matrix of the test joints was occurred during the dwell time at the high temperature as in the thermally aged SAC alloys [62,63]. Considering that the test joints spent 250 hours at the 125 °C per 1000 cycles, the insignificant growth of IMC particles

was very well in consistence with results achieved from the Sn3.8Ag0.7Cu and Sn4Ag0.5Cu solder joints aged at the same temperature [62,63].

4.1.2 SAC-In joints

After the first reflow, the as-soldered SAC-In joints with large initial grains (Fig. 7a) have the similar metallurgical features as reported in Paper IV. The solder matrix consisted of tin and indium where the In-content varies mainly around 3 at%, which is under the solubility limit of indium in tin. Silver formed intermetallic compounds (IMC) with tin and indium. The size of these particles varied from less than 1 μm to up to 5 – 7 μm. The composition of this IMC type was approximately 75 at% Ag, 18 at% Sn and 7 at% In corresponding to the $Ag_3(Sn,In)$ compound. The result was consistent with findings in the Sn9In3.5Ag0.5Cu solder after reflow although the indium content of the IMC is lower in this study [64]. The $Ag_3(Sn,In)$ particles was not evenly distributed in the solder matrix, but they often formed clusters. The absence of the fine dispersed Ag_3Sn particles that were typically detected in the solder matrix of the near-eutectic SnAgCu alloys (Fig. 9c) was evident. Moreover, Suhling et al. [65] identified phases containing only silver and indium in Sn8In3Ag0.5Cu solder. These were not observed by Sharif and Chan [64] or in Paper IV. Copper reacted also with tin and indium forming either up to 5 μm long elongated or small (> 1 μm) spherical phases $Cu_6(Sn_{1-x}In_x)_5$ in the SAC-In solder. According to EDS analysis, at-% fractions of Cu:Sn:In were 51:46:3, respectively, being in consistent with the findings made by Sharif and Chan, who studied the Sn9In3.5Ag0.5 Cu alloy [64].

Comparing with the microstructure of the Sn9In3.5Ag0.5Cu solder [64], the only major exception was the existence of the sigma phase ($InSn_4$) in the microstructure of the SAC-In joints after reflow soldering (Table 7), as shown in Fig. 9b. However, formation of a sigma phase in indium-containing lead-free solders was reported in literature [66,67]. This was due to segregation of indium during cooling in some ternary SnInAg alloys, resulting in an excess amount of indium in the liquid [66,67]. It was also shown that the solid-state phase transformation $\beta Sn+In \rightarrow \beta Sn + \gamma\ (InSn_4)$ in binary Sn8In and Sn10In alloys occurred at the high temperatures of 125 °C - 150 °C [68]. In paper IV, the indium content after non-equilibrium solidification of the SAC-In joints was significantly lower (2 - 3 wt%) than the nominal 7 wt% due to the formation of $Ag_3(Sn,In)$ and $Cu_6(Sn,In)_5$ particles. This was less than the maximum solubility of indium in tin at 150 °C [69], suggesting that no phase transformation occurred during the TCT. Moreover, the $\gamma\ (InSn_4)$ phase could not be detected from the matrix after the test. Thus, it was concluded that the phase transformation $\beta Sn+In\ solute \rightarrow \beta Sn + \gamma(InSn_4)$ did not occur in the test joints during the TCT and, consequently, the $\gamma(InSn_4)$ phase in the as-soldered microstructure had no major effect on the thermal fatigue behavior of the SAC-In joints [Paper IV].

The SEM/EDS also indicated that the indium content in the slightly coarsened IMC particles was homogenized during the TCT [Papers II and IV]. Suhling et al. [65] observed that coarsening of the IMC particles occurred in the Sn8In3Ag0.5Cu joints of resistors (2512) during the TCT, although no quantitative analysis of the composition of the IMC

particles and the Sn matrix was given. It must be noted, however, that the size and distribution of the IMC particles in the initial microstructure of the Sn8In3Ag0.5Cu joints in Ref. 65 did not correspond with the as-soldered microstructure of the SAC-In joints with the nominal Ag content of 4.1 wt%. Furthermore, the low Ag content in the Sn9.5In1.5Ag0.7 Cu resulted in the formation of the $Ag_2(Sn,In)$ particles instead of the $Ag_3(Sn,In)$ particles [70]. Abovementioned results suggested that the Ag content had a major effect on the solidified microstructure in 6 - 9 wt% In-containing lead-free solders similarly with ternary SAC alloys.

In the case of extremely harsh TCT conditions (–55 °C - 150 °C), the indium content of the solder matrix was under the reliable detection limit of the EDS analysis. The decreased indiumn content was due to the coarsening of the $Ag_3(Sn,In)$ particles during the TCT (Table 8). This observation was in accordance with the results of earlier studies [24, Paper II], although the phenomenon did not occur to such a degree in those test joints. It was assumed that the diffusion rate of the indium atoms in the test joints was increased by the higher upper temperature extreme (150 °C) and increased strain due to the larger global thermal mismatch of the assembly, since these altered conditions of the joint will likely result in an increased amount of dislocations and vacancies in the Sn matrix.

4.1.3 Interaction between solders and metallizations of LTCC module

A thin (2-3 μm) Ag_3Sn layer was formed at the metallization/solder interface after reflow soldering in all AgPt (QS 264) metallized test modules with ternary SAC solders [Papers I,III,IV]. No excessive growth of the IMC layer was detected after the TCT. This is in consistence with the other studies in which the interactions between this metallization and lead-free solders was reported [15,24,29,40,42,71,72]

According to the SEM/EDS analysis (Fig. 9a), the IMC layer (average layer thickness 2 μm - 4 μm) composition of $Ag_3(Sn_{1-x}In_x)$ formed between the AgPt (QS 264) metallization and the SAC-In solder after ball attachment [Papers II and IV]. This was similar to earlier findings in AgPt (QS 264) metallization/SAC-In solder interfaces [24,40]. The average thickness of 5 μm - 7 μm was determined after the TCT over a temperature range –55 °C - 150 °C, whereas the lesser growth of the IMC layer was observed after the milder TCTs over temperature ranges of 0 °C - 100 °C and –40 °C - 125 °C [Papers II and IV]. Thus, the growth of the IMC layer was not excessive in any test conditions used of this study.

Considering the metallurgy of the ENIG/solder interface on the LTCC side of the joint, the $(Cu,Ni)_6Sn_5$ layer was observed in the SAC387 joints after soldering at the typical reflow peak temperatures similarly with the other studies focusing on the interactions between ternary SAC alloys and ENIG deposition [73-87]. On the other hand, a TEM investigation of the as-soldered Sn1Ag0.5Cu and Sn4Ag0.5Cu joints proved that a thin layer of $(Ni,Cu)_3Sn_4$ may exist between the Ni deposit and $(Cu,Ni)_6Sn_5$ layer after reflow soldering [83]. The SEM investigation also showed that the IMC layers of SAC405 and SAC387 did not grow noticeably during the TCT. This is due to the nickel barrier pre-

venting the diffusion of copper from the pad to the IMC layer. Thus, no extra copper was available for the growth of the IMC layer. The composition of the IMC layer remained practically unaltered during the TCT, although phase transformations $(Cu,Ni)_6Sn_5 \rightarrow (Ni,Cu)_3Sn_4$ was reported after the thermal aging in the relatively high temperatures (≥ 150 °C) [76,81,88]. Furthermore, the formation of the Cu_3Sn layer between Cu_6Sn_5 and copper layer of the PCSB was detected, but this did not had an effect on the primary failure mechanisms of the test joint, as discussed in Chapter 4.3.

The IMC layer of the ENIG plated SAC-In joint (Fig. 9d) did not contain indium after reflow soldering, contrary to the observations of small (3 - 6 at%) indium content in the IMC layer between Sn9In3.5Ag0.5 Cu solder and Au/NiP metallization [89-92]. This was probably due to the lower peak temperature of the present reflow processes compared with 240 °C - 250 °C temperatures used in the other studies. However, indium was detected in the IMC layer after the TCT, and the indium content in $Ag_3(Sn,In)$ and $Cu_6(Sn,In)_5$ particles within the solder matrix was slightly increased, similar to the SAC-In joints of AgPt-metallized modules [Papers II and IV]. Therefore, the detected phase transformationd did not degrade the reliability of the present ENIG plated test joints.

4.2 Recrystallization of test joints

It is well established that recrystallization occurs in thermomechanically loaded collapsible BGA joints of ternary SAC alloys [48-51,54]. On the other hand, no clear evidence of recrystallization in Sn3.8Ag0.7Cu specimens was detected in the isothermal cycling tests at various temperatures [93,94]. On this basis, it was concluded that recrystallization is not inherent property of the alloy, but it is related to constrained stress conditions of BGA joints [94]. Similarly, no occurrence of recrystallization in this alloy was observed in thermal cycling test of lap joint specimens at various temperatures or in TCT over a temperature range of RT - 100 °C [95,96]. On the other hand, Lauro et al. [97] showed that recrystallization and grain growth occurred in a bulk Sn3.5 Ag and Sn3.5Ag.0.5Cu samples (∅ 0.2 in., height 0.125 in.) after compressive deformation of 30% and subsequent annealing (48h, 150 °C), whereas Sn0.7Cu required only compressive deformation of 20%. Furthermore, Vianco et al. [98] reported that both static and dynamic recrystallization occurred in Sn3.9Ag0.6Cu specimens during isothermal time-independent stress/strain tests. Thus, the recrystallization seems to occur in various Sn-based solders if the stress/strain conditions are adequate.

Considering the recrystallizion process of the lead-free BGA joints, it was reported that the subgrains formed within the initial large grains before the new recrystallized microstructure was formed at the strain concentrated locations of Sn based lead-free BGA solder joints [49,54,79]. The initiation of the several intergranular microcracks could occur in low angle grain boundaries [49,79], but the final crack will propagate along the grain boundaries of the recrystallized microsturcture [48-51,54]. It was also shown that relatively high (≥ 3 wt%) Ag content resulted in suppressed grain growth in the recrystallized SnAg0.5Cu solder matrix during the TCT over a temperature range of –40 °C - 125 °C compared with the low (≤ 2 wt%) Ag content. It was assumed that the pinning effect of

fine Ag_3Sn dispersions resulted in suppressed grain growth in SAC alloys [48,99,100]. Moreover, Gong et al. [101] stated that Ag_3Sn particles could prevent the propagation of the sub-boundaries in Sn3.5Ag0.7Cu alloy. Finally, Sundelin et al. [49] showed that the hypoeutectic Sn3Ag0.5Cu solder recrystallized more readily than the SAC387 and SAC405 solders. They also concluded that this difference was related to the lower amount of Ag_3Sn particles in the hypoeutectic solder. Thus, the Ag-content seemed to have a major effect on the solidified microstructure, as discussed in 4.1.1, and its recrystallization and subsequent coarsening during the TCT in ternary SAC alloys. On this basis, it can be assumed that there was no significant difference between the recrystallization of SAC387 and SAC405 solders in the test assemblies used in this study, since the Ag-contents of these solder were almost equal.

The nature of the grain boudaries can also affect the recrystallization behavior of the lead-free solders, since Terashima et al. [49,99,100] reported that notably greater amount of the low energy coincidence site lattice (CSL) boundaries existed in the Sn3Ag0.5Cu and Sn1.2Ag0.5Cu0.05Ni solders compared with the Sn1Ag0.5Cu after the TCT over a temperature range of –40 °C - 125 °C. On this basis, it was suggested that the sufficient amount of the low energy special boundaries (twin and other CSL boundaries) could diminish the number of the continuous connections between individual random boundaries and, consequently hinder the advantageous sites for crack propagation. Finally, Henderson et al. [50] stated that the scale of the recrystallized zone may depend on the local crystallographic orientation of the Sn matrix and on the applied stress field, and it may vary significantly from joint to joint.

Hence, the recrystallization of Sn based BGA solder joints seems to depend on stress/strain distribution of the joint and the initial microstructure after solidification. Furthermore, the anisotropic features of Sn based solders may cause variation in recrystallization kinetics among individual joints. Besides these factors, the different solder land materials may have an influence on the recrystallization behviour of the lead-free BGA joints due to the dissolution of solid deposit. Mattila et al. [51] stated that dissolution of copper from Cu pad to the ternary SAC solders resulted in formation of large primary Cu_6Sn_5 particles during reflow soldering. These particles enhanced the nucleation in recrystallization process and, consequently, caused faster formation of the recrystallized region within the joints compared with the joints soldered on AuNi deposit. Although Cu pads were not used in this study, it seemed evident that the dissolution of copper from PCSB to liquid solder occurred in some extent the during reflow processes. This is due to the fact that the amount of dissolved Cu atoms was enough to cause the formation of the $(Cu,Ni)_6Sn_5$ layer on the ENIG plated pads in Sn36Pb2Ag solder joint with PCSB [8]. However, no significant difference between the microstructures of the collapsible and non-collapsible joints was observed, as mentioned in Chapter 4.1.1. The reasons for this were probably the lesser dissolution of copper due to the lower (≈230 °C) reflow peak temperature used in this study compared with the 240 °C - 245 °C temperature range used in Ref. 51 and the formation of $(Cu,Ni)_6Sn_5$ layer, which consumed excess copper from the liquid solder.

Finally, the nucleation of recrystallization occurs more easily close to voids, since they are localization sites of internal stresses in the solder joints [54]. Therefore, severe voiding next the solder/component interface will probably cause faster recrystallization of the solder in this high stress/strain region of the BGA joint and, consequently, faster initiation of the intergranular cracking compared with BGA joint with no excessive voiding. However, the X-ray investigation indicated that no excessive voiding occurred in the test assemblies.

The results of optical microscopy with polarized light proved that recrystallization occurred in the joints of the test assemblies B - D (Fig. 8). This was quite expected, since the higher stress/strain distributions probably existed in the critical joints of the present test assemblies compared with the test assemblies used in Refs. 48 - 51 and 54 due to the large global thermal mismatch LTCC/PWB assemblies and the relatively large component size. Moreover, the results suggested that the SAC-In joints were more prone to recrystallization than the SAC387 and Sn3Ag0.5In0.05Ni joints [Papers IV and V]. In other words, more energy was stored in the SAC-In joints in similar joint configurations due to inelastic deformation compared with the other test solders. This in turn suggested that the plasticity of the SAC-In solder was higher, especially at low temperatures, than the plasticity of the other test solders. On the other hand, the amount of cumulative deformation varied in the different test joints due to the different number of thermal cycles. Thus, the present observations did not prove categorically the assumption of higher plasticity of SAC-In solder at a low temperature. Unfortunately, no studies focusing on the recrystallization behaviour or temperature dependent mechanical properties of SnInAgCu alloys can be found in literature. Therefore, more information about the recrystallization kinetics of the SAC-In solder and its plasticity is obviously required.

4.3 Failure mechanisms of thermomechanically loaded solder joints

The importance of knowing the exact failure mechanisms of lead-free solder joints with respect to reliable lifetime estimation was stated in the literature [61,102], although the results achieved from the limited accelerated tests in the laboratory conditions do not necessarily correspond exactly to the reliability of solder joints in field conditions. Nevertheless, the need for models to use in simulating strain/stress distribution in solder joints and, consequently, estimating lifetime duration of solder joints in different microelectronic packages is obvious. These models require not only the temperature-dependent material parameters of the assembly, but also the TCT data to determine acceleration factors and to verify the results of simulations. Moreover, the reliability models are typically based on the assumption of creep deformation in solder joints. Obviously, such model cannot predict accurately the lifetime of the electronic packages in which a different primary failure mechanism has caused the failure of the second level interconnections.

Considering the present test assemblies, the SAM analyses proved that the separate cracks were propagating from the outer and inner edges towards the centre of the joint in all of them. Generally, the global thermal mismatch between a component with BGA joints and a PWB is assumed to induce compressive stresses at the outer edge of the BGA

joints on the component side at the high temperature extreme and tension stresses at the low temperature extreme during the TCT [103]. Obviously, the simplified stress conditions are inversed at the inner edge of the joint. Therefore, it can be concluded that the crack located in the inner edge of the critical test joints was formed at the high temperature extreme and the one observed in the outer edge of the joints was formed at the low temperature extreme. The detailed failure analysis of the test joint configurations is given below.

4.3.1 SAC405 and SAC387 solders

The FE-SEM analysis clearly showed the occurrence of intergranular cracking in the outer edge of the non-collapsible SAC405 joints tested in the mild TCT over a temperature range of 0 °C - 100 °C (Fig. 16). In other words, the primary failure of this joint was related to creep. The fraction of separated IMC/solder interface in the inner edge of the joints was decreased compared with the harsher TCT conditions [Paper I]. However, the primary failure mechanism in the outer edge of the joint changed when the temperature swing of the TCT was increased.

The main characteristic features of the outer fracture surface in the SAC405 joints after the TCT over a temperature ranges of –40 °C - 125 °C and –55 °C - 150 °C were presented in Fig. 17. The observations presented in Figs. 8 and 11c suggested that localized recrystallization occurred in the critical area of the joint (i.e. the location of high strain energy density) during the TCT over a temperature range of –40 °C - 125 °C similarly with localized recrystallization detected in the higher deformation regions of the various SAC solder joints tested over a temperature range of –40 (or –45) °C - 125 °C [48-51,54]. Furthermore, there were several intergranular cracks on the fracture surface, indicating severe creep-related damage (Fig. 17). Another characteristic feature was the existence of fatigue striations, proving that the thermally induced failure also propagated in a transgranular manner due to thermal fatigue, as shown in Fig. 17. The occurrence of the thermomechanically induced mixed transgranular and intergranular failure in Sn-xAg-0.5Cu (x = 1 – 4 wt%) solder in the temperature range of –40 - 125 °C and in the isothermal fatigue test of the Sn3Ag0.5Cu alloy with the high stress ratio of 0.7 was reported earlier, although no fractographic analysis of the test specimens was given in these studies [48,104].

An approximately 200 - 300 μm wide zone with a coarser grains existed next to the fine recrystallized zone (enlarged in Fig. 17c). Unfortunately, no optical microscopy investigation with polarized light was conducted in Paper I, but based on the discussion of the previous Chapter, it can be assumed that recrystallization behavior of SAC387 and SAC405 solders was quite similar. The zone consisting the coarse grains was probably a consequence of thermal strain-induced recrystallization and subsequent grain growth during thermal cycling, although it was assumed in Paper I that the failure located outside the recrystallized zone. Nonetheless, the latter assumption is not quite improbable, since Yang et al. [59] has shown recently that small grains next to the pad of a BGA joint could be detected in an OIM (Orientation Imaging Microscopy) map, although these grains

were not visible in the micrograph of the same joint obtained using polarized light microscopy. It is also generally known that relatively fine equiaxial grains can form next to the solid surface in the beginning of the solidification process before the subsequent dendritic solidification of the remaining melt.

The striations were clearly wider in this zone with a coarser microstructure compared with the fine-grained zone (Fig. 17). Generally, the width of a single striation indicates the distance that the crack propagates during one cycle in a high stress intensity factor range (ΔK), but in the case of a low ΔK the formation of one striation might take several cycles. Although no reliable calculation for ΔK can be made due to a lack of temperature-dependent material parameters for the PCSB, the results suggested that the propagation rate of a thermomechanical fatigue/creep crack increases noticeably after a certain critical crack length, since the average width of the striation is approximately 0.25 μm and 1.25 μm in the recrystallized zone and the zone with coarse microstructure, respectively [Paper I].

On the basis of the above, it was proposed that the mixed intergranular/transgranular failure initiated in the SAC405 joints at low temperature extreme occurs in three stages [Paper I]. In the first stage, inelastic deformation concentrated in the critical area of the joint (i.e. the region of the highest strain energy density) causes recrystallization. Afterwards, the failure is formed in the recrystallized zone mainly by grain boundary sliding and, to a lesser extent, by transgranular fatigue cracking. When the failure has propagated through the fine recrystallized zone, the primary failure mechanism is changed. The next stage is mainly governed by transgranular (fatigue) cracking. Furthermore, the rate of crack propagation is noticeably increased in the third stage due to increased stress intensity at the crack tip and the coarser microstructure.

Moreover, the observations of FE-SEM analysis (Fig. 18) proved that a mixture of transgranular (fatigue) and intergranular (creep) failures formed also in the SAC387 joints at the low temperature extreme, similar to the joints of AgPt-metallized SAC405 joints. However, the decreased width of the striations on the fracture surface of the SAC387 joints showed better fatigue endurance compared with SAC405 alloy. No specific explanation could be given for this difference on the basis of the present results. Generally, the different thermal fatigue endurance of the ternary SAC alloys is related to the characteristic features of the solidified microstructure of these alloys, since the fraction, size, distribution and stability of the IMC particles within the solder matrix had a significant effect on the thermal fatigue endurance of the ternary SAC alloys. Furthermore, it was suggested that the sufficient amount of the low energy special boundaries (twin and other CSL boundaries) could diminish the number of the continuous connections between individual random boundaries and, consequently decrease the advantageous routes for crack propagation, since the high energy random orientated boundaries are more favourable sites for intergranular cracking [99,100]. Therefore, a thorough investigation into the recystallzation behaviour of these solders in the thermally induced high stress/strain conditions would be required in order to clarify this issue.

The SEM analyses (Figs. 11 and 12) also confirmed that the separation of the IMC/solder interface of the AgPt metallized modules could be eliminated using the ENIG deposition in the LTCC module. Moreover, the results also showed significant inelastic deformation and subsequent formation of the separate intergranular failure between the via and the PCSB (Fig. 12). This is in accordance with the simulated stress distribution of PCSB joints showing the highest stress level in the same region (i.e. the centre region of the component/joint interface) [16,105]. Thereby, it was proved that intergranular cracking could exist within the solder matrix between the PCSB and via before the cracks propagating towards this region from the inner and outer edges reached it.

Considering the collapsible SAC405 joints, the SEM and FE-SEM investigations of the test joints proved that intergranular creep was the dominant failure mechanism at the outer edge of the joints in the LTCC/Arlon assembly in the TCT over a temperature range of –40 °C - 125 °C (Figs. 10 and 14). This was in accordance with the observations concerning the thermal fatigue behavior of ternary SAC alloys in the BGA joints of ceramic, flip-chip, and CSP packages during thermal cycling tests over a temperature range of –40 (or –45) °C - 125 °C [48-51,54]. On the other hand, clear indications of transgranular fatigue cracking were noticed at the outer edge of the collapsible SAC405 joints in the LTCC/FR-4 assembly (Fig. 15). The transgranular (fatigue) failure was also observed in the non-collapsible SAC405 joints of the assembly A after the TCT over a temperature range of –40 °C - 125 °C [Paper I]. Thereby, the dominant failure mechanism of thermal fatigue in the SAC405 solder was dependent on the induced stress level in the temperature range of –40 °C - 125 °C. All the above-mentioned results showed that not only the temperature but also the stress level had a strong influence on the dominant failure mechanism in the thermomechanically loaded SAC405 solder.

4.3.2 SAC-In solder

The FE-SEM analysis (Fig. 19) showed that primary failure mode at the both edges of the AgPt and ENIG metallized SAC-In joint was the intergranular (creep) cracking in the TCTs over temperature ranges of 0 °C - 100 °C and –40 °C - 125 °C [Papers II and V]. It was shown in Fig. 7a that the initial solidified microstructure of the SAC-In joints consisted only a few large grains. Thus, the fine grain size of the fractured surfaces was assumed to be a consequence of inelastic deformation and subsequent recrystallization of the joint [Papers II and V]. Furthermore, the narrow recrystallized zone of the SAC405 joints did not exist in this joint, but the grain size of the fractured surface within the region of the intergranular cracking seemed to vary from 5 μm to 10 μm (Figs. 19b-d). This was notably finer grain size compared with the grain size of the coarsened zone in the SAC405 joints, shown in Fig. 17a. This indicated that the growth rate of the recrystallized grains was slower in the SAC-In solder compared with the SAC405 alloy. This can probably explain why the transgranular fracture did not existed in the SAC-In joints in these TCT conditions, since it is known that the grain boundaries of the fine-grained microstructure can resist the transgranular cracking compared with the coarse grain structure. In the Paper II, it was assumed that indium alloying was the basic reason for the finer grain size and, consequently, to the absence of the transgranular cracking, since the

Ag_3Sn particles were coarser in the SAC-In solder compared with the SAC405 solder. However, the assumption is not necessarily valid, since the suppressed grain growth can also be consequence of the low energy grain boundaries in Sn based lead-free solders, as was discussed in Chapter 4.2.

Moreover, the creep resistance of SAC-In solder seemed to be better than that of SAC387 solders at elevated temperatures, since the intergranular crack was formed at the high temperature extreme within the recrystallized zone of the joints, but the lifetime of the SAC-In joint were significantly higher compared with the SAC387 joint [Papers II and V]. A possible explanation for the enhanced creep resistance of the SAC-In solder was suggested in Paper IV. Based on the results that the rate-limiting creep mechanism in pure tin and in three SAC alloys was core-diffusion-controlled dislocation climb and the activation energy Q_{core} in Sn and ternary alloys was 42 kJ/mol and 61 kJ/mol, respectively, it was assumed that the difference in Q_{core} values was related to segregation of Ag and Cu atoms near the dislocation cores in saturated βSn [106]. Therefore, it was suggested that indium atoms may have a similar effect on dislocation movements in the βSn phase of SAC-In solder as do Ag and Cu atoms in SAC alloys, since the higher solute atom volume would probably increase the Q_{core} value in indium-containing solder compared with SAC alloys [Paper IV]. Consequently, more external energy would be required to activate dislocation climb in SAC-In solder, and its creep resistance would be better at elevated temperatures, resulting in better lifetime duration of SAC-In compared with other Sn-based lead-free solders tested in non-collapsible joints with PCSB [71, Papers I and V].

Unfortunately, no study on the activation energies and creep mechanisms of SAC-In solder is found in the literature to verify or refute the assumption presented in Paper IV. Moreover, it must be noted that abovementioned results have been achieved from the testing of the non-recrystallized specimens, whereas the recrystallization of the BGA joints changes the situation during the TCT in real solder joints. Thus, it is more likely that indium atoms delay the recrystallization and the subsequent initiation of the intergranular (creep) cracking within the solder matrix. Finally, the EDS analysis showed that the indium content in the tin matrix decreased significantly during the TCT over a temperature range of –55 °C - 150 °C (Tables 7 and 8). It is therefore possible that the favorable effect of the indium alloying on creep resistance of the solder also decreases during thermomechanical loading.

The transgranular failure formed in the SAC-In joints during the extremely harsh test conditions over a temperature range of –55 °C - 150 °C (Fig. 20), but the width of the striations (Figs. 17d and 20b) proved that the propagation rate of the transgranular crack was notably slower in SAC-In solder compared with SAC405 joints tested in the same conditions. Thus, it was concluded that the fatigue resistance of SAC-In solder was higher compared with SAC405 solder and, consequently, it was one reason for the better lifetime duration of the test assembly with SAC-In joints. Finally, the results presented in Papers II and IV proved that the failure mechanisms of the SAC-In joints depended on the temperature range and the magnitude of the global thermal mismatch, similarly to the ternary SAC joints, but the occurrence of transgranular cracking in the SAC-In solder

joint required higher stress/strain conditions compared with the other non-collapsible Sn based lead-free solder joints with PCSB.

4.3.3 Ceramic and ceramic/metallization interface failures

This failure type is considered to be the disadvantageous failure type, since it can not be detected using DC measurements and, consequently, the life-time of the joint can not be estimated with reasonable accuracy [5,9,12-15,40,42]. Moreover, if the LTCC module is subjected to both thermal and mechanical stresses, such as vibration, the reduced mechanical strength of the joint configuration due to cracking in the ceramic might cause a failure long before the estimated failure time of the device has been reached.

Considering the occasional failures at the ceramic/metallization interface in the test module with sintered Ag based metallization, the occasional cracks in the ceramic/joint interface of the LTCC package shown in Fig. 5 could been observed after 100 cycles or later, whereas the typical primary overload induced ceramic cracking were observed before 100 cycles in the TCT over a temperature range of –40 ° C - 125 °C [9,12-15,40]. This means that the initiation and propagation of these cracks were slower compared with the ceramic cracking observed in the AgPd metallized LTCC modules and AgPt metallized ones without the solder mask.

The SAM analyses showed that the joint of the test assemblies C and E suffered from the primary cracking in the ceramic or the ceramic/metallization interface (Table 6). However, the ENIG plated test structures were capable to absorb the thermally induced stresses sufficiently and they suffered less from the failures within the ceramic and at the ceramic/metallization interface compared with the Sn3Ag0.5Cu0.5In0.05Ni joints [Paper V]. Nevertheless, the relatively poor adhesion between the Ag-base metallization (Du Pont 6154) and LTCC (Du Pont 951) indicates that there is still need for improvement of the adhesion strength of the LTCC/metallization pairs in future. Recent advancement in this matter has been reported in literature [107,108].

4.3.4 Failures related to PCSB

A different failure mechanism of the BGA joints related to the plastic core solder balls in various packages was reported earlier. In these studies, a crack in the copper layer in the middle of the PCSB (∅ ≤ 500 μm) in ceramic packages soldered to organic PWBs was observed [10,16,25,109-111]. It was assumed that the maximum thermal stress in the PCSB is located near the centre of the sphere, regardless of the high strain regions near the solder/pad interfaces [16,25]. On the other hand, this failure mechanism did not occur in the present test assemblies [Papers I, II, IV and V], in the other LTCC/PWB assemblies with the 800 μm or 1100 μm PCSBs [8,40,71,72], or in more flexible assemblies with the small PCBSs (∅ ≤ 500 μm) [26,112-114].

Furthermore, it was suggested that solder cracking of the non-collapsible joint with PCSB was due to the excessive amount of solder in the joint [10,109,110]. The excessive amount of solder, in turn, was supposed to reduce the elasticity of the PCSB joint to the same level with the ordinary collapsible BGA solder sphere [110]. In surface mount technology, however, the typical stencil thicknesses are 125 μm, 150 μm and 180 μm. Since solder paste contains approximately 50 vol% of metal particles, the solder volume after the paste printing and the reflow soldering can be calculated. Assuming that the ball diameter, the stencil aperatures, and the size of the solder lands are equal, the ratio of the polymer and solder volumes (V_{PCSB}/V_{solder}) can also be calculated. Hence, with the typical stencil thicknesses (180 μm - 125 μm) and the ball diameter of 300 μm, 500 μm, 800 μm, and 1100 μm this ratio varies within the range of 1.7 - 2.5, 3.3 - 4.7, 5.1 - 7.3, and 7.3 - 10.5, respectively. Naturally, the thin (20 μm) copper layer on the polymer core increase the stiffness of sphere in some extent, but still the assumption of similar elasticity of the non-collapsible solder joint with PCSB and the conventional collapsible or non-collpsible BGA solder joints due to the excessive amount of solder seems very unrealistic, especially in the case of a large (800 μm or 1100 μm) PCSB. In fact, over 75 % increase in characteristic lifetime was achieved in the LTCC/PWB assembly with 800 μm spheres after the TCT over a temperature range of –40 °C - 125 °C when the 90Pb10Sn spheres was replaced with the PCSBs [8]. Overall, it can be assumed that cracking in the copper layer in the middle of the PCSB can be avoided in the given test/field conditions using standard SMT procedures, the combination of a properly designed joint structure, and a suiTable area array in the BGA packages.

4.4 Effect of failure mechanism on lifetime of test assemblies

The thermomechanically induced failures of the ternary SAC-BGA joints are generally associated with the inelastic deformation in the solder matrix due to creep. The superior creep properties of the bulk SAC alloys due to dispersion strengthening of Ag_3Sn and Cu_6Sn_5 particles compared with the SnPb alloys in the isothermal creep tests were reported [115,116], but the accelerated testing of the actual solder joints revealed that the thermal fatigue endurance of SAC solder joints were poorer compared with the lead containing solder joints in the certain test conditions, as mentioned in Chapter 1. The degradation of the creep resistance of the SAC joints was concluded to be consequence of the coarsening of IMC particles [117].

However, the creep resistance in metals is also dependent on the grain size. This factor is usually neglected in the modelling of the reliability of the solder joints and it is commonly assumed that the fraction of plastic deformation is negligible compared with the fraction of creep deformation in the total amount of the inelastic strain of the BGA joint [118]. In practice, however, the amount of accumulated strain due to the plastic deformation during the TCT is sufficient to cause recrystallization in the lead-free BGA joints. Thus, the recrystallization kinetics of the lead-free solder affects evidently thermal fatigue endurance of the lead-free BGA solder joint, whereas the anisotropic nature of Sn based lead-free solders causes variations in the thermal fatigue endurance of the joints. In fact, Andersson et al. [119] showed that the area of the fractured surfaces in the thermally

cycled Sn3.8Ag0.7Cu BGA joints was not identical despite of the similar DNPs (distance to neutral point) of the joints. This means that the crack growth rate probably varied also in the present test joints resulting in variations between the lifetimes of the test modules.

4.4.1 Non-collapsible BGA joints

The thermal cycling test results of the comparable LTCC/PWB assemblies with 800 μm PCSBs are compiled in Table 14.

Table 14. Characteristic lifetime θ and Weibull shape factor β values of the different non-collapsible BGA joints with 800 μm PCSB tested over a temperature ranges of –40 °C - 125 °C and 0 °C - 100 °C.

Temperature range of −40° C - 125 °C			
Joint configuration	**θ**	**β**	**Ref.**
Sn36Pb2Ag/PCSB/ Sn36Pb2Ag	1378	7.9	8
Sn2.8Ag0.8Cu0.5Sb/PCSB/SAC405*	983 cycles	4.0	69
Sn3Ag0.5Cu0.5In0.05Ni /PCSB/SAC405	826 cycles	8.7	69
SAC-In	1432 cycles	5.3	Paper II
SAC405	917 cycles	6.8	Paper I
E-SAC387*	957 cycles	7.1	PaperV
E-SAC-In*	1371 cycles	6.2	PaperV
E-Sn3Ag0.5Cu0.5In0.05Ni	1368 cycles	8.1	PaperV
H-SAC387	1835 cycles	10.1	PaperV
H-SAC-In	2325 cycles	9.0	PaperV
Temperature range of 0° C - 100 °C			
Joint configuration	**θ**	**β**	**Ref.**
Sn36Pb2Ag/PCSB/ Sn36Pb2Ag	3952	11.1	8
SAC-In /PCSB/SAC405	5590	6.3	Paper II
SAC405/PCSB/SAC405	4298	5.4	Paper I

* primary failure mechanism: ceramic cracking

The data given in Table 14 showed notably better thermal fatigue endurance of the SAC-In joints compared with the other lead-free joints when only solder cracking existed in the test joints. The lifetime of SAC-In joint was also at the same level with the lead-containing joint in the harsh test conditions. This proved that the problems related to the ternary SAC solders in the elevated temperatures and high thermal stress conditions can be avoided applying SAC-In solder to the joint configuration. Overall, it can be concluded that the lead-free non-collapsible solder joints with the PCSB in the LTCC modules can be made using either the SAC or SAC-In alloys, if the required thermal fatigue endurance is specified in relatively mild test conditions (e.g. temperature range of 0 °C - 100 °C). If the test specification of the LTCC application requires harsher test conditions, the SAC405, SAC387, Sn3Ag0.5Cu0.5In0.05Ni, and Sn2.8Ag0.8Cu0.5Sb solders cannot be used in the LTCC/PWB assemblies with a large global thermal mismatch.

It was evident that the difference between the characteristic lifetimes of the joints also depended on the rigidity of the assembly. Although the coefficient of thermal expansion (CTE) and the flexural strength were comparable for both systems (5.8 and 315 MPa for Du Pont 951; 6.1 and >200 MPa for HL2000; 5.5 and 290 MPa for CT800) [7,120,121], the thickness of the Du Pont 951 modules was over 70% greater than that of the

CT800/HL2000 modules, resulting in a more rigid assembly in ENIG plated test sets. Thus, the increased characteristic lifetime of test assembly D was due to thinner LTCC modules compared with test assembly C similarly with the results of the other studies in which the effect of the in thickness in the ceramic packages was studied [122,123].

The promising results of the TCTs indicated that adequate lifetime duration could be achieved in relatively thin LTCC assemblies using either SAC387 or SAC-In solder with PCSB, whereas the use of SAC-In solder was preferable in thicker modules in order to achieve a preferred 1000 cycles in the TCT over a temperature range of - 40 °C - 125 °C [44]. The use of SAC-In solder on the LTCC side of the composite joint proved to be a potential solution for further design of a reliable second-level solder interconnection in LTCC/PWB assemblies under severe test conditions. This was shown recently in the TCT test over a temperature range of –40 °C - 125 °C of the LTCC-SiP package for telecommunication applications [72]

The lifetimes of the three different joint configurations in the test assembly C (ENIG plated Du Pont 951 modules) were not comparable with the other results due to the different primary failure mechanisms (Table 12). As mentioned earlier, ceramic cracking is known to cause inaccuracy in the determination of the characteristic lifetime and it was therefore deemed to be an unaccepTable failure mechanism in LTCC modules. The high characteristic lifetime of the modules with Sn3Ag0.5Cu0.5In0.05Ni was most likely due to ceramic cracking similar to that found in AgPd-metallized LTCC modules [Paper V]. On the other hand, it seemed that the failures of the SAC387 and SAC-In modules in the teset assembly C were detected adequately. This was due to the fact that a few critical joints (i.e. a corner joint or the joints next to it) that failed within the solder matrix existed in these modules [Paper V]. This and the data of Table 14 suggest, in turn, that there was no significant difference between the characteristic lifetimes of AgPt and ENIG-deposited modules of test assemblies A and C. Therefore, preventing of the separation between the IMC layer and the solder matrix seemed to have no major effect on the characteristic lifetime of the LTCC/PWB assemblies contrary to the assumption that the elimination of this failure mode would be one of the key factors contributing to the enhanced lifetime of the lead-free non-collapsible solder joint in the harsh test condition [Paper II].

Considering the reliability of the test assembly B tested in the extremely harsh conditions (–55 °C - 150 °C), the first failure occurred after 588 cycles in the SAC-In joints [Paper IV]. This cycle number passed the limit of 500 cycles of NTC-B, but was notably lower than the limit of 1000 cycles (NTC-C) preferred in the TCT over a temperature range of –55 °C - 125 °C [44]. The SAC405 joint did not pass the limit of 200 cycles (NTC-A). However, comparing the reliability of these test joint configurations with the requirements of the IPC-9701 standard is not unambiguous, since the TCT over a temperature range of –55 °C - 150 °C does not belong to the test conditions mentioned in the IPC-9701 standard [44].

As discussed in Chapter 4.3.2, it seems evident that SAC-In solder can resist transgranular (fatigue) and intergranular (creep) cracking better than other tested lead-free solders in

high stress/strain conditions that exist in LTCC/PWB assemblies with a large global thermal mismatch (CTE ≥ 10 ppm/°K). This can be also seen from the data shown in Table 13. Furthermore, Suhling et al. [65] proved the beneficial effect of indium on thermal fatigue endurance by exposing different sized chip resistors to a thermal cycling test over a temperature range of –40 ° C - 150 °C. In these test conditions, the characteristic lifetime of Sn8In3Ag0.5Cu solder was almost 2.5 times longer than that of Sn3.8Ag0.5Cu, whereas the difference between the lifetimes of these solder joints was not significant in the milder TCT. Therefore, it can be concluded that the 7 - 9 wt% In containing quaternary Sn based solders have the notably enhanced thermal fatigue endurance in the case of the high stress/strain distribution within the solder joint compared with the ternary SAC solders, whereas this difference between the solders is lesser in the moderate stress/strain conditions of the solder joint [65, Papers I,II,IV,V].

In the perspective of the reliability modelling of the present test assemblies with PCSBs, the SAC405, SAC387, Sn3Ag0.5Cu0.5In0.05Ni, or Sn2.5Ag0.8Cu0.5Sb solder joints are inapplicable, since the primary failure mechanism is not pure creep, but mixed transgranular/intergranular cracking and separation of the IMC/solder interface occurred in these joints in the harsh test conditions (–40 °C - 125 °C) [71,72,Papers I,II,IV,V]. In the case of the SAC-In joint, the failure is related to creep in the typical test conditions of the telecommunication applications [Paper II], since the change of the primary failure mechanism of the joint occurred in the extremely harsh conditions (–55 °C - 150 °C) [Paper IV]. Therefore, the primary failure mechanism of the SAC-In joint seemed to be suiTable for most lifetime estimation models.

4.4.2 Collapsible BGA joints

The SAM and SEM analyses proved that primary ceramic cracking occurred in the modules of the LTCC/FR-4 assembly under the harsh test conditions (Table 6 and Fig. 10a). Otherwise, the failures were located either at the IMC/solder interface or in the solder matrix in the other test assemblies, as shown in Fig. 10b. In the case of the LTCC/FR-4 assembly under the harsh test conditions, it was evident that the stress level exceeded the fracture strength of the LTCC material, resulting in ceramic cracking.

Theoretically, the basic methods for avoiding ceramic cracking in the collapsible joints of the LTCC/PWB assemblies with a high global thermal mismatch are to increase the strength, elasticity, and stand-off height of the joint configuration. According to Jones et al. [7], Dupont 951 had the highest fracture strength in 3- and 4-point bending tests among six commercial LTCC tape materials. This means that finding an LTCC material with notably higher fracture strength may currently be difficult. On the other hand, selecting a lead-free tin-based solder material with higher elasticity and significantly better creep/fatigue properties compared with SAC405 solder is probably a difficult task. Furthermore, increasing the height of a collapsible solder sphere to match, for example, a 0.8 - 1.0 mm stand-off height with the same aspect ratio would require an impractical initial sphere size of approximately ∅2 mm [Paper III].

Finally, the data shown in Table 13 proves that the characteristic lifetime of collapsible SAC405 solder joints in LTCC/FR-4 assemblies did not reach the characteristic lifetime of non-collapsible joints with PCSB in the mild TCT over a temperature range 0 °C - 100 °C. The SEM analysis clearly indicated the occurrence of intergranular creep cracking in the joints tested in the mild TCT over a temperature range of 0 °C - 100 °C [Paper III]. This proved that the primary failure mechanisms of the collapsible SAC405 and non-collapsible SAC405/PCSB solder joints can be the same, but the higher stand-off height and enhanced elasticity due to the PCSB in the latter joint configuration resulted in a longer characteristic lifetime compared with the former joint (Tables 11-13). It was therefore concluded that a collapsible lead-free solder joint is not a feasible option in LTCC/PWB assemblies with a high global thermal mismatch [Paper III]. However, comparing the data shown in Table 13 with typical industrial specifications [124], it can be assumed that collapsible SAC405 joints would be a potential choice for LTCC/PWB assemblies with a low global thermal mismatch in a few cases.

4.5 Design aspects of reliable interconnections

First of all, it is important to realize that both the RF and reliability performance requirements related to the 2nd level solder joints must be taken into account simultaneously when a surface-mounTable LTCC module for high-frequency applications is designed. Otherwise, the 2nd level solder interconnections may have excellent RF properties but inadequate reliability or visa versa. It would also be beneficial in an economic sense to design a set of generic, reliable module platforms suitable for use in a wide range of high-speed digital and RF/wireless applications instead of developing and qualifying customized LTCC RF module packages for each product. This would also provide a significant reduction in the product development time and associated costs [72]. Obviously, it is essential to design a reliable 2nd level solder joint configuration for such platform set. This will allow the packaging designer to utilize common low-cost substrate materials without sacrificing the assembly reliability.

The surface-mounTable LTCC-SiP modules can be attached onto a PWB using BGA, LGA or CGA interconnection methods, as mentioned in Chapter 1.1. It was shown that non-collapsible 9010PbSn spheres, collapsible lead-free BGA or LGA joints were not reliable solution for the large LTCC modules (15 mm x 15 mm) in the assemblies with large global thermal mismatch between the module and the PWB [24,29,Paper III]. In the case of CCGA packages, the thin columns are difficult to process, since they bend easily and require special tooling [25]. Therefore, the non-collapsible BGA joint with the PCSB seems to be the most promising choice for the 2nd level interconnections of the large LTCC module platforms. The PCSBs can also provide predicTable RF characteristics since they maintain their stand-off height during reflow-soldering process. Furthermore, conducted full-wave electromagnetic simulations have shown that the polymer core has no degrading impact on RF/microwave performance of the BGA package [8,25]. The changes in thermal performance of the PCSB are also small compared with eutectic BGA solder joints [26].

In the RF design perspective, the use of large BGA joints means that they inherently have larger interconnection reactances (i.e. capacitance and inductance), which ultimately determine the upper frequency limit of the wideband RF BGA transition structure [125]. One possible way to mitigate the unwanted effect associated with the larger BGA joints is to incorporate an air-cavity in the vicinity of the RF signal pad [11]. Moreover, it was shown that the air-cavity structure did not have an adverse effect on the reliability of the 2nd level solder interconnections. Thus, the utilization of the air-cavity structure in LTCC RF module applications can be recommended [72].

In practice, an LTCC application may require leaving sufficient space for a RF BGA transition structure, or placing components on the module backside surface (i.e. along with BGA joints). In these cases, the necessary transition from full BGA matrix to partial area-array or peripheral BGA joint configuration will ineviTable result in the increased stress level in the joints and, consequently, the decreased characteristic lifetime of the module assembly in the typical TCT conditions. In these cases, the partial array should be as symmetric as possible in order to avoid the excessive stress and accumulation of inelastic deformation in the critical joints of the asymmetric matrix [72].

4.5.1 Design of solder lands in LTCC module

The thick film printed solder lands of a LTCC module are often fabricated using silver or silver based metallization, although other commercial options are also available. It was shown that silver based metallizations (AgPd and AgPt) reacted with tin faster than silver [35]. Moreover, increasing Pd (1 wt%, 5 wt%, and 15 wt%) or Pt (1 wt%and 5 wt%) content increased the rate of IMC growth by Sn diffusion into the silver based metal plate [35]. Considering the proper solder land of the LTCC module, the use of metallization material that is prone to leaching must be avoided, since the leaching will most likely cause ceramic cracking in LTCC/PWB assemblies [9,12-15,40]. Therefore, the leaching tendency of the sintered silver based metallizations should be investigated before the metallization is accepted to the LTCC products.

As mentioned in Chapter 1, the transition from lead-containing solders to lead-free solders is predicted to cause more severe leaching of thick film metallizations during soldering [18]. This is due to the higher temperatures required in soldering and the higher tin content of the lead-free solders. In the typical fabrication of the LTCC/PWB assembly the metallization of the LTCC module is exposed to two reflow cycles. An average thickness of 12 - 16 μm seems to be adequate for the proper Ag based metallizations, if excessive IMC growth can be avoided during reflow soldering [40,126].

Dissolution at the solid/liquid interface is governed by the surface area of the solid and the volume of the liquid, as stated in the Nearns-Brenner equation. The roughness of fired metallization naturally increases the surface area of the solder lands. It has been pointed out that fired metallization is a porous material layer, and liquid solder will flow into the pores due to capillary force and, consequently, degrade the reliability of the LTCC module [18,38-40]. Thus, the roughness and porosity of the thick film increases the effective

area between liquid solder and solid LTCC metallization and results in faster dissolution of the initial metallization layer during the soldering process. Therefore, the porosity of sintered thick films should be minimized in order to inhibit the leaching of Ag-based thick films. This can be achieved to some extent with optimal co-firing process. Porosity is, however, a consequence of the metal ratio and binder contents of the metallization. Thus, pastes should be designed to produce a dense metallization layer after the co-firing process [40].

In practice, the solderability of the Ag-based metallization may cause severe voiding and, consequently, reliability problems in the LTCC/PWB assemblies. For example, early failures were detected in the DC measurements of an LTCC-SiP/PWB assembly containing the Ag metallized modules with SAC-In joints after 600 cycles. The explanation of these failures was shown in Fig. 21. Extremely large voids existed on the LTCC side of the joint enabling a fast propagation of the primary crack within the solder joint. The formation of the excessive large voids in the SAC-In joints of the Ag metallized modules was due to the incompatible flux system of the solder. The large voids was seen also in the Sn7In4.1Ag0.5Cu joints of the 15 mm x 15 mm LTCC modules with relatively low (950 cycles) characteristic lifetime [127]. On the basis of the vendor's recommendation [128], the problem was solved using the solder paste with improved flux system. This prevented the excessive voiding in the similar AgPt and ENIG metallized modules and the failures were located within the solder matrix [72].

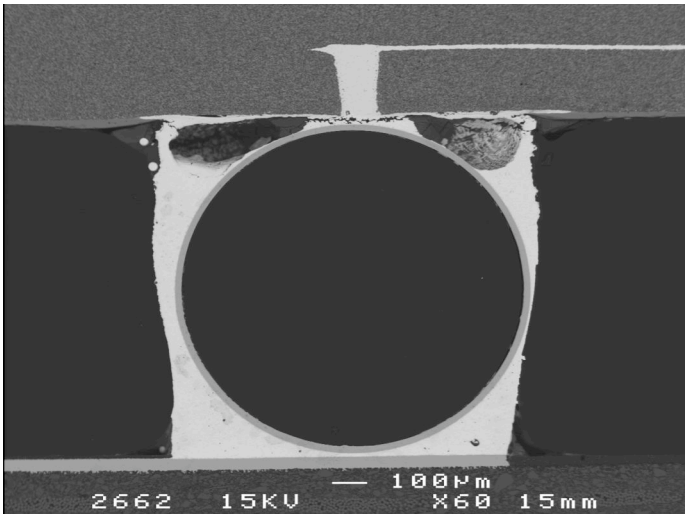

Fig. 21. Large voids in the Ag metallized SAC-In joint.

Moreover, the use of Ag metallization in Sn3Ag0.5Cu0.5In0.05Ni joints caused prolonged separation between Ag_3Sn layer and solder matrix in the LTCC-SiP package (Fig. 22). The substantial voiding at the LTCC/joint interface observed in non-destructive investigation of the assembly (Fig. 5) had probably accelerated the growth rate of the crack formed at the Ag_3Sn/solder interface in the inner edge of the Ag metallized joint. Thus, the notably lower characteristic lifetime of these joints compared with the similar AgPt metallized LTCC package in Ref. 72 was probably a consequence of the prolonged sepa-

ration between the IMC layer and solder matrix. It was also recently shown that the Sn3Ag0.5Cu0.5In0.05Ni solder is more prone to voiding on the Ag-based metallization compared with the ternary 95.5Sn4Ag0.5Cu [29]. Thus, it seemed obvious that the Sn3Ag0.5Cu0.5In0.05Ni alloy and its flux system used in Refs. 29, 71, and 72 was not optimum for the Ag based metallization of the LTCC modules. This short case study was include in this thesis in order to demonstrate how important it is to verify the compliance of the solder/metallization pair in the LTCC applications.

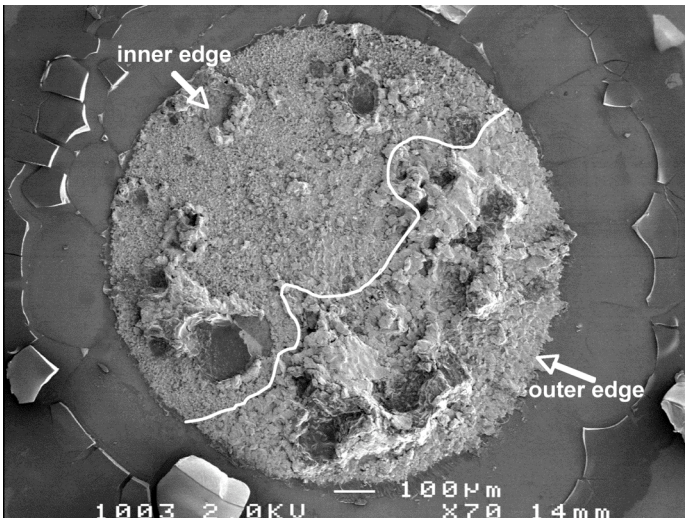

Fig. 22. Fracture surfaces on the LTCC side of the Ag metallized Sn3Ag0.5Cu0.5In0.05Ni joints formed during the thermal cycling test over a temperature range of –40 °C - 125 °C.

The results indicated that the harmful effect of the dissolution and inadequate solderability of the Ag-based metallization on the reliability of the LTCC modules can be avoided using ENIG deposition. Being a common deposition material without glass phase to degrade the solderability of the solder lands, it is more compatible with the commercial lead-free solder pastes compared with Ag based metallizations. Furthermore, the separation of the IMC/solder interface can be prevented using ENIG deposit [Paper V]. On the other hand, it is generally known that the "black pad" phenomenon is related to ENIG deposition. Although this phenomenon did not occur in this study, the possibility of its occurrence in commercial LTCC should be considered during the design and material selection of the LTCC module. It was also shown that the plating process might cause cracking in the ceramic solder mask (Fig. 6).

In order to summarize the relevant aspects of material selection for LTCC applications, the advantages and disadvantages of ENIG- and Ag-based metallizations in LTCC applications are compiled in Table 15.

Table 15. Characteristic features of ENIG and Ag based metallizations in LTCC applications [Paper V].

Deposit	Advantages	Disadvantages
Ag based metal-	• Matched with LTCC	• Excessive leaching may occur

lizations	tapes • No need for extra plating process	• Adverse effect of glass phase on solderability • Inadequate adhesion strength between ceramic and metallization may exist
ENIG	• No leaching • Good solderability	• Extra plating process is required • Cracking of ceramic solder mask during ENIG plating process may occur • Inadequate adhesion strength between ceramic and Ag metallization may exist • Black pad phenomenon may occur

Although the selection of the proper metallization material for the solder lands of the LTCC module is essential in the design of the reliable 2nd level solder joint configuration, another main requirement for the reliable 2nd level interconnections of LTCC modules is the sufficient adhesion between ceramic and metallization. For this reason, a solder mask printed on the metallized solder land is needed to prevent ceramic cracking or the detachment of the metallization [5,15,42]. The use of the solder mask provides more beneficial stress distribution in the outer edge of the BGA joint (i.e. region with high stress during the TCT) due to the larger area of the ceramic/metallization interface compared with the non-solder mask joints [5,15,42]. In this study, ∅1.0 and ∅1.2 mm solder lands with 0.8 mm solder mask opening were used. This means that the overlaps of about 0.1 mm and 0.2 mm existed in the solder joint configurations. The larger diameter was applied in order to enhance the adhesion strength of the ceramic/metallization interface. Moreover, the yield of the LTCC modules will also increase due to the wider tolerances in solder mask alignment during the printing process [Paper V]. On the other hand, too large signal pad size may deteriorate the RF performance and reduce the upper cut-off frequency limit of the broadband RF BGA transition structure in a BGA joint used for a RF signal connection [72].

Considering the adequate adhesion strength of the ceramic/joint interface in an LTCC application, it is worth mentioning that the results achieved from the isothermal tests are only indicative. For example, the adhesion strength of the AgPd metallization may be in the adequate level, but the metallization itself is not feasible for the 2nd level interconnections due to leaching, as mentioned before. The stress level at ceramic/joint interface also depends on many variables (temperature, package size, BGA matrix, solder material, etc.). For example, the use of Sn3Ag0.5Cu0.5In0.05Ni solder caused severe ceramic cracking in the ENIG plated test modules, whereas more failures within the solder matrix was detected in the critical SAC387 and SAC-In solder joints in the similar assemblies [Paper V]. Therefore, the adequacy of the LTCC/metallization/solder combination should be verified case-specifically.

4.5.2 Selection criteria for solder material

The primary cracking within the solder was located on the LTCC side in the non-collapsible solder joint configuration of the LTCC/PWB assemblies [4,5,8,9,24,40,42,71,72, Papers I,II,IV,V]. Therefore, the enhancement of the thermal fatigue endurance in the upper half of the non-collapsible joint is one of the key factors in

the design of the reliable 2nd level interconnections. In this study, the SAC-In solder had the best characteristic lifetime and favourable failure mechanisms compared with other lead-free solders (Tables 12 and 14). In the perspective of industrial manufacturers, the required soldering process of an LTCC application has to match with the normal reflow parameters for lead-free products. The results proved that the use of two lead-free solders with different liquidus temperatures in this joint configuration did not cause problems during the reflow process, although the T_l of SAC-In was approximately 10 °C lower than the T_l of SAC405 solder, an X-ray inspection proved that no excessive soldering defects occurred in the joints of the test assemblies, despite the different liquidus temperatures.

Because of the relatively high price of indium and the general cost-efficiency requirements of the electronics industry [129], a new low-indium alloyed and nickel-doped pentanary Sn3Ag0.5Cu0.5In0.05Ni solder was applied into one test module set with the ENIG deposited metallization [Paper V]. Since the mechanical properties of solder alloys, like strength and Young's modulus, are typically temperature-dependent factors, the excessive ceramic cracking of the joints with Sn3Ag0.5Cu0.5In0.05Ni solder suggested that this solder resulted in the highest stress levels at the interface between ceramic and metallization compared with E-SAC387 and E-SAC-In joints [Paper V]. This indicated, in turn, that Sn3Ag0.5Cu0.5In0.05Ni solder had the best resistance against inelastic deformation at the low temperature extreme. However, it can be assumed that a solder alloy, in which strength and plasticity do not change notably with decreasing temperature, would be a more favourable choice for lead-free joint configurations in LTCC/PWB assemblies, since it would reduce the increasing stress level within the critical region of the joint configuration (i.e. ceramic/joint interface) at low temperatures and, consequently, eliminate the failures related to the ceramic and/or the ceramic/metallization interface.

Overall, the results presented in this study proved that a manufacture of the SAC-In solder joint configuration should not have any major technical limitations in terms of common industrial fabrication methods and at the moment the SAC-In solder is the most promising candidate to guarantee the adequate thermal fatigue endurance in the LTCC/PWB assemblies with large global thermal mismatch.

5 Conclusions

The characteristic features of thermomechanically induced failures in the lead-free collapsible and non-collapsible BGA joints applied to the LTCC/PWB assemblies with high global thermal mismatch were determined in this study. The main results and conclusions can be listed as follows:

1. The results showed that the collapsible SAC405 joint configuration is not feasible option in the LTCC/PWB assemblies with high global thermal mismatch due to its inadequate lifetime in the mild TCT over a temperature range 0 °C - 100 °C and its tendency to cause ceramic cracking in the module during the TCT over a temperature range –40 °C - 125 °C.

2. The non-collapsible SAC405 joint showed better thermal fatigue endurance in the TCT over a temperature range 0 °C - 100 °C compared with the lead-containing joint configuration with PCSB. The primary failure mechanism of the SAC405 joint was intergranular (creep) cracking. However, in the TCT over a temperature range –40 °C - 125 °C, two different failure mechanisms were detected in the non-collabsible SAC405 joints with AgPt metallization. A mixed transgranular/intergranular failure formed within the solder matrix in the outer edge of the joint at the low temperature, whereas separation of the IMC/solder interface existed in the inner edge of the joint. In the case of the ENIG plated modules, the adhesion between the IMC layer and solder matrix was sufficient to hinder the separation of this interface, resulting in the formation of an intergranular failure within the solder matrix at the high temperature extreme. Finally, the failure analysis of collapsible SAC405 sphere proved that the primary failure mechanisms of SAC405 solder depend on the stress level of the BGA joint.

3. At least two separate cracks were formed in the critical SAC-In joints at the temperature extremes of the TCTs over temperature ranges of 0 °C - 100 °C and –40 °C - 125 °C. These cracks propagated in the SAC-In solder matrix and their characteristic features were mostly related to the features of intergranular (creep) fracture. Due to the better creep/fatigue endurance of SAC-In solder and higher characteristic lifetime compared with other tested lead-free solders, this joint configuration is assumed to be a promising solution for the further design of the reliable 2^{nd} level solder interconnection in LTCC/PWB assemblies with a high global thermal mismatch for telecommunication applications.

4. Mixed transgranular/intergranular failure existed in the SAC-In joints in the extremely harsh test conditions over a temperature range of –55 °C - 150 °C, but the growth rate of the crack was significantly lower compared with SAC387 joints tested in the same conditions. This proved that the failure mechanisms of the SAC-In joints depended on the temperature range and the magnitude of the global thermal mismatch, similar to the ternary SAC joints, but the occurrence of trans-

granular cracking in the SAC-In solder joint required higher stress/strain conditions compared with the ternary SAC joints.

5. A sTable IMC layer was formed between the Ni deposit and the solder matrix during reflow soldering. The layer thickness did not grow excessively during the TCT over a temperature range of –40 °C - 125 °C. Thus, the reliability problems related to leaching of Ag-based metallization in LTCC applications could be avoided using ENIG deposition. It was shown, however, that preventing of the separation between the IMC layer and the solder matrix seemed to have no major effect on the characteristic lifetime of the LTCC/PWB assemblies.

6. The use of two lead-free solders with different liquidus temperatures in the non-collapsible BGA joint configuration did not cause problems during the reflow process. Moreover, the typical reflow process did not result in any adverse phenomenon on the LTCC side of the AgPt and ENIG plated SAC-In joints. Therefore, the manufacture of these solder joint configurations should not have any major technical limitations in terms of common industrial fabrication methods.

References

1. Heyen J, Kerssenbrock T, Chernyakov A, Heide P & Jacob AF (2003) Novel LTCC/BGA modules for highly integrated millimeter-wave transceivers. IEEE Transactions on Microwave Theory and Technology 51(12): 2589 - 2596.

2. Lee J-H , DeJean G, Sarkar S. Pinel S, Lim K, Papapolymerou J, Laskar J & Tentzeris MM (2005) Highly integrated millimeter-wave passive components using 3-D LTCC system-on-packages (SOP) technology. IEEE Transaction on Microwave Theory and Technology 53(2): 2220 - 2229.

3. Kangasvieri T, Halme J, Vähäkangas J & Lahti M (2008) Low-loss and broadband BGA package transition for LTCC-SiP applications. Microwave and Optical Technology Letters 50(4): 1036 - 1040.

4. Cho YS, Needes CR, Souders KE, Hang KW, Donohue PC, Niblett AR & Amey DA (2000) LTCC ceramic components on printed wiring boards - The issues and potential solutions. In: Proceedings of the 2000 International Symposium on Microelectronics, Boston, USA: 665-668.

5. Prabhu A, Schafer WJ & Patil S (2000). High reliability LTCC BGA for telecom applications. In: Proceedings of the 26th IEEE/CPTM International Electronics Manufacturing Technology Symposium, Santa Clara, USA: 311 - 323.

6. Imanaka Y (2005) Multilayered low temperature cofired ceramics (LTCC) technology. Springer Science + Business Media, Boston, USA.

7. Jones WK, Liu Y, Larsen B, Eang P & Zampino M (2000), Chemical, structural and mechanical properties of the LTCC tapes. In: Proceedings of International Symposium on Electronics, Boston, USA: 669 - 675.

8. Kangasvieri T, Nousiainen O, Putaala J, Rautioaho R & Vähäkangas J (2006) Reliability and RF performance of BGA solder joints with plastic-core solder balls in LTCC/PWB assemblies. Microelectronics Reliability 46(8): 1335 - 1347.

9. Rautioaho R, Nousiainen O, Leppävuori S & Vähäkangas J (2002) Reliability of solder joints in LTCC/PCB assemblies. In: Procceedings of the European Microelectronics Packaging & Interconnection Symposium, Cracow, Poland: 153 - 158.

10. Schwanke D, Haas T, Zeilmann C, Halser K & Klein M (2003) Reliability investigations of BGA-interconnections between RF-LTCC-modules and PCBs. In: Proceedings of 14th European Microelectronics and Packaging Conference, Friedrichshafen, Germany: 213 - 218.

11. Fu C-Y & Huang R-F (2000) BGA reliability of multilayer ceramic integrated circuit (MCIC) devices. The International Journal of Microcircuits and Electronic Packaging, 23(4): 393-399.

12. Rautioaho R, Nousiainen O, Saven T, Leppävuori S & Lenkkeri J (2000) Thermal fatigue and metallurgical reactions in solder joints of LTCC modules, Microelectronics Reliability 40(8-10): 1527 - 1532.

13. Rautioaho R, Nousiainen O, Leppävuori S, Lenkkeri J & Jaakola T (2001) Thermal fatigue in solder joints of Ag-Pd and Ag-Pt metallized LTCC modules. Microelectronics Reliability 41(9-10): 1643 - 1648.

14. Rautioaho R, Nousiainen O, Leppävuori S, Vähäkangas J (2003) Dimple BGA joint structure and reliability in LTCC / PCB assemblies. In: Proceeding of the 14th European Microelectronics and Packaging Conference, Friedrichshafen, Germany: 29 - 33.

15. Nousiainen O, Rautioaho R, Kautio K, Jääskeläinen J & Leppävuori S (2005) Solder joint reliability in AgPt-metallized LTCC modules. Soldering & Surface Mount Technology 17(3): 32 - 42.

16. Okinaga N, Kuroda H & Nagai Y (2001) Excellent reliability of solder ball made of a compliant plastic core. Proceedings of the 51st Electronic components and Technology Conference, Orlando, USA: 1345 - 1349.

17. Mawer A, Dopplinger A & Mercer B (2005) Application Note: Manufacturing with the land grid array package. Freescale Semiconductor, Doc. no. AN2920: 1-12.

18. Vianco PT (2001) Pb-free solder alloy development and intermetallic compound layer growth in high-reliability hybrid microcircuits. The International Journal of Microcircuits and Electronic Packaging 24(4): 328 - 345.

19. Bartelo J, Cain SR, Caletka D, Darbha K, Gosselin T, Hendersson DW, King D, Knadle K, Sarkhel A, Thiel G, Woychik C, Shih DY, Kang S, Puttlitz K & Woods J (2001) Thermomechanical fatigue behavior of selected lead-free solders. In: Proceedings of the IPC SMEMA Council APEX 2001, San Diego, CA, USA: LF2-2 1 - LF2-2 12.

20. Clech J-P (2004) Lead-free and mixed assembly solder joint. Reliability trends. In: Proceedings of the IPC Printed Circuits Expo, Anaheim, CA, USA: S28-3-1 - S28-3-14.

21. Salmela O, Andersson K, Särkkä J & Tammenmaa M (2005) Reliability Analysis of some ceramic lead-free solder attachments. Proceedings of Pan Pacific Microelectronics Symposium Conference, Kauai, Hawaii, USA: 161 - 169.

22. Qi Y, Lam R, Ghorrbani HR, Snugovsky P & Spelt JK (2006), Temperature profile effects in accelerated thermal cycling of SnPb and Pb-free solder joints. Microelectronics Reliability 46(2 - 4): 574 - 588.

23. Yang SY, Kim I & Lee S-B (2008) A study on the thermal fatigue behavior of solder joints under power cycling conditions. IEEE Transactions on Components and Packaging Technologies, 31(1): 3 - 12.

24. Nousiainen O, Putaala J, Kangasvieri T, Rautioaho R & Vähäkangas, J. (2006) Metallurgical reactions in composite 90Pb10Sn/lead-free solder joints and their effect on reliability of LTCC/PWB assembly. Journal of Electronic Materials 35(10): 1857 - 1865.

25. Movva S & Aquirre G (2004) High reliability second level interconnects using polymer core BGAs. In: Proceedings of the 54th Electronic Components and Technology Conference, Las Vegas, NV, USA: 1443 – 1448.

26. Galloway J, Syed A, Kang W, Kim J, Cannis J, Ka Y, Kim S, Kim T, Lee G & Ryu S (2005) Mechanical, thermal, and electrical analysis of a compliant interconnect. IEEE Transactions on Components and Packaging Technology 28(2): 297-302.

27. Farooq M, Goldsmith C, Jackson R & Martin G. (2003) Lead-free ceramic ball grid array: thermomechanical fatigue reliability. Journal of Electronic Materials 32(12): 1421 - 1425.

28. Maeda K, Higashi M, Kokubu M & Nakagawa, S. (2000) The application of HITCE ceramic material for LGA-type chip scale package. In: Proceedings of 2000 Electronic Components and Technology Conference, Las Vegas, USA: 358 - 363.

29. Nousiainen O, Urhonen T, Kangasvieri T, Rautioaho R & Vähäkangas J (2010) Thermomechanically loaded lead-free LGA joints in LTCC/PWB assemblies. Soldering & Surface Mount Technology 22(2): 21 - 29.

30. Ghaffarian R (2006) Ball grid array reliability assessment for aerospace applications. Microelectronics Reliability 46(12): 695 - 706.

31. Directive 2002/95/EC of the European Parliament and of the council of the 27 January 2003 on the restrictions of the use of certain hazardous substances in electrical and electronic equipment.

32. Park SB, Joshi R & Goldmann L (2004) Reliability of lead-free copper columns in comparison with tin-lead solder column interconnects. In: Proceedings of the 54th Electronics Components and Technology Conference, Las Vegas, USA: 82 - 89.

33. Interrante M, Coffin J, Cole M, De Sousa I, Farooq M, Goldmann L, Goldsmith C, Jozwiak J, Lopez T, Martin G, Truong VT & Welsh D (2003) Lead-free package interconnections for ceramic grid arrays. In: Proceedings of the 28th International Electronics Manufacturing Technology Symposium, San Jose, USA: 85 - 92.

34. Park SB & Joshi R Microelectronics Reliability (200b) Comparison of thermo-mechanical behavior of lead-free copper and tin-lead column grid array packages. Microelectronics Reliability 48(5): 763 - 772.

35. Yamada K, Makuta F & Chiba S (1992) Degradation of soldered thick film conductor during thermal cycling. In: Proceedings of the ISMH '92, Reston, USA: 725 - 730.

36. Zhong ZW, Arulvanan P, Maw PH & Lu CWA (2007) Characterization of SnAgCu and SnPb solder joints on low-temperature co-fired ceramic substrate. Soldering & Surface Mount Technology 19(4): 18 - 24.

37. Tian D & Kutilainen T (2003) Microstructures in solder joints between Sn95.5Ag4Cu0.5 solder and Ag/Pd thick film. Journal of Electronic Materials 32(3): 152 - 158.

38. Erickson KL, Hopkins PL & Vianco PT (1998) Modelling the solid-state reaction between Sn-Pb solder and a porous substrate coating. Journal of Electronic Materials 27(11): 1177 - 1192.

39. Cheng MD, Wang SS & Chuang TH (2002) Soldering reactions between In49Sn and Ag thick films. Journal of Electronic Materials 31(3): 171 - 177.

40. Nousiainen O, Kangasvieri T, Rönkä K, Rautioaho R & Vähäkangas J (2007) Interfacial reactions between Sn-based solders and AgPt thick film metallizations on LTCC. Soldering & Surface Mount Technology 19(3): 15 - 26.

41. Bochenek A, Bober B, Dziedzic A & Golonka L (2001) Investigations of assembly properties of conductive layers in LTCC circuits. Microelectronics International 18(2): 11 - 15.

42. Nousiainen O, Putaala J, Kangasvieri T, Rautioaho R & Vähäkangas J (2006) Design and characterization of composite solder joint in LTCC/PWB assembly. In: Proceedings of the IMAPS Nordic Annual Conference, Gothenburg, Sweden: 161 - 165.

43. Hwang JS (2001) Environment-friendly Electronics: Lead-free Technology. Electrochemical Publications, Port Erin, Isle of Man.

44. Performance test methods and qualification requirements for surface mount solder attachments, IPC-9701, 2002.

45. Temperature cycling, JEDEC Standard No. 22-A104C, 2005.

46. Semmens JE & Kessler LW (1997) Characterization of flip chip interconnect failure modes using high frequency acoustic micro imaging with correlative analysis. In: Proceedings of the 5th Annual IEEE International Reliability Physics Symposiums, New York, NY, USA: 141 - 148.

47. Nousiainen O, Rautioaho R, Leppävuori S, Uusimäki A & Tian D (2001) Acoustic micro imaging of fatigue cracking in solder joints of LTCC modules. In: Proceedings of the 13th European Microelectronics and Packaging Conference, Strasbourg, Belgium: 172 - 177.

48. Terashima S, Kariya Y, Hosoi T& Tanaka M (2004) Effect of silver content on thermal fatigue life of Sn-xAg-0.5Cu flip-chip interconnects. Journal of Electronic Materials 32(12): 1527 - 1533.

49. Terashima S, Takahama K, Nozaki M & Tanaka M (2004) Recrystallization of Sn grains due to thermal strain in Sn-1.2Ag-0.5Cu-0.05Ni solder. Materials Transaction 45(4): 1383 - 1390.

50. Hendersson DW, Woods JJ, Gosselin TA, Bartelo J, King DE, Korhonen TM, Korhonen MA, Lehman LP, Cotts EJ, Kang SK, Lauro P, Shih D-Y, Goldsmith C & Puttliz KJ (2004) The microstructure of Sn in near-eutectic Sn-Ag-Cu alloy solder joints and its role in thermomechanical fatigue. Journal of Materials Research 19(6): 1608 - 1612.

51. Mattila TT, Vuorinen V & Kivilahti JK (2004) Impact of printed wiring board coatings on the reliability of lead-free chip-scale package interconnections. Journal of Materials Research 19(11): 3214 - 3223.

52. LaLonde A, Emelander D, Jeanette J, Larson C, Rietz W, Swenson D & Hendersson DW (2004) Quantitative metallography of β-Sn dendrites in Sn-3.8Ag-0.7Cu ball grid array solder balls via electron backscatter diffraction and polarized light microscopy. Journal of Electronic Materials 33(12): 1545 - 1549.

53. Lu HY, Balkan H & Ng KYS (2006) Effect of Ag content on the microstructure development of Sn-Ag-Cu interconnects. Journal of Materials Science: Materials in Electronics 17(x): 171 - 188.

54. Sundelin JJ, Nurmi TT & Lepistö TK (2008) Recrystallization behaviour of SnAgCu solder joints. Materials Science and Engineering A 474(1-2): 201 - 207.

55. Sylvestre J & Blander A (2008) Large-scale correlations in the orientation of grains in lead-free solder joints. Journal of Electronic Materials 37(10): 1618 - 1623.

56. Berthou M, Retailleau P, Frémont H, Guédon-Gracia A & Jéphos-Davannel C (2009) Microstructure evolution observation for SAC solder joint: Comparison between thermal cycling and thermal storage. Microelectronics Reliability 49(9-11): 1267 - 1272.

57. Mueller M, Wiese S, Roellig M, & Wolter K-J (2007) The dependence of composition, cooling rate and size on the solidification behaviour of SnAgCu solders. In: Proceedings of EuroSimE 2007, London, UK: 446 - 455.

58. Wiese S, Roellig M, Mueller M & Wolter K-J (2008) The effect of downscaling the dimensions of solder interconnects on their creep properties. Microelectronics Reliability 48(6): 843 - 850.

59. Yang S, Tian Y & Wang C (2010) Investigation on Sn grain number and crystal orientation in the Sn-Ag-Cu/Cu solder joints of different sizes. Journal of Materials Science: Materials in Electronics DOI 10.1007/s10854-009-0042-x

60. Reid M, Punch J, Collins M & Ryan C (2008) Effect of Ag content on the microstructure of Sn-Ag-Cu based solder alloys. Soldering & Surface Mount Technology 20(4): 3 - 8.

61. Dutta I, Pan D, Marks RA & Jadhav SG (2005) Effect of thermo-mechanically induced microstructural coarsening on the evolution of creep response of SnAg-based microelctronic solders. Materials Science and Engineering A 410-411: 48.

62. Fix AR, Nüchter W & Wilde J (2008) Microstructural changes of lead-free solder joints during long-term ageing, thermal cycling and vibration fatigue. Soldering & Surface Mount Technology 20(1): 13 - 21.

63. Pang JHL, Low TH, Xiong BS, Xu L & Neo CC (2004) Thermal cycling effects on Sn-Ag-Cu solder joint microstructure, IMC and strength. Thin Solid Films 462-463: 370 - 375.

64. Sharif A & Chan YC (2005) Effect of indium addition in Sn-rich solder on the dissolution of Cu metallization. Journal of Alloys Compounds 390(1-2): 67-73.

65. Suhling JC, Gale HS, Johnson RW, Islam MN, Shete T, Lall P., Bozack MJ, Evans JL. Seto P, Gupta T & Thompson JR (2004) Thermal cycling reliability of lead-free chip resistor solder joints", Soldering & Surface Mount Technology 16(2): 77 - 87.

66. Korhonen T-M & Kivilahti JK (1998) Thermodynamics of the Sn-In-Ag solder system. Journal of Electronic Materials 27(3): 149 - 158.

67. Song J-M, Wu Z-M & Huang D-A (2007) Two-stage nonequilibrium eutectic transformation in a Sn-3.5Ag-3In solder. Scripta Materilia 56(5): 413 - 416.

68. Kim K-S, Imanishi T, Suganuma K, Ueshima M & Kato R (2007) Properties of low temperature Sn-Ag-Bi-In solder system. Microelectronics Reliability 47(7): 1113 - 1119.

69. Hansen M (1958) Constituition of binary alloys. McGraw-Hill, New york, USA.

70. Sopousek J, Palcut M, Hodulova E & Janovec J (2010). Thermal analysis of the Sn-Ag-Cu-In solder alloy. Journal of Electronic Materials 39(3): 312 - 317.

71. Nousiainen O, Kangasvieri T, Rautioaho R & Vähäkangas J (2010) Sn3Ag0.5Cu0.5In0.05Ni and Sn2.5Ag0.8Cu0.5Sb solders in composite solder joints of LTCC/PWB assemblies. Accepted to Soldering & Surface Mount Technology.

72. Nousiainen O, Kangasvieri T, Rautioaho R & Vähäkangas J (2010) Reliability study of lead-free non-collapsible BGA joints in an LTCC package for RF/microwave telecommunication applications. Unpublished paper.

73. Luo W-C & Kao CR (2002) Liquid/solid and solid/solid reactions between Sn-Ag-Cu solders and Ni surface finish. In Proceedings of the 4th International Symposium on Electronic Materials and Packaging, Kaohsiung, Taiwan: 330 - 334.

74. Zribi A, Clark A, Zavalij L, Borgesen P & Cotts CJ (2002) The growth of intermetallic compounds at Sn-Ag-Cu solder/Cu and Sn-Ag-Cu solder/Ni interfaces and the associated evolution of the solder microstructure. Journal of Electronic Materials 30(6): 1157 - 1164.

75. Kim KS, Huh SH & Suganuma K (2003) Effects of intermetallic compounds on properties of Sn-Ag-Cu lead-free soldered joints. Journal of Alloys Compounds 352(1-2): 226 - 236.

76. Cheng MD, Chang SY, Yen SF & Chuang TH (2004) Intermetallic compounds formed during the reflow and aging of Sn-3.8Ag-0.7Cu and Sn-20In-2Ag-0.5Cu solder ball grid array packages. Journal of Electronic Materials. 33(3): 171 - 180.

77. Kim S-W, Yoon J-W & Jung, S-B (2004) Interfacial reactions and shear strengths between Sn-Ag based Pb-free solder balls and Au/EN/Cu metallization. Journal of Electronic Materials. 33(11): 1182 - 1189.

78. Nurmi S, Sundelin J, Ristolainen E & Lepistö T (2004) The effect of solder paste composition on the reliability of SnAgCu joints. Microelectronics Reliability 44(3): 485 - 494.

79. Dunford S, Canumalla S & Viswanadham P (2004) Intermetallic morphology and damage evolution under thermomechanical fatigue of lead (Pb)-free solder interconnections. In: Proceedings of the 2004 Electronics and Technology conference, Las Vegas, USA: 726 - 736.

80. Li D, Liu C & Conway PP (2006) Interfacial reactions between Pb-free solders and metallised substrate surfaces. In: Proceedings of the 6th International Conference on Electronic Packaging Technology, Shenzhen,China: 360 - 365.

81. Sun P, Andersson C, Wei X, Cheng, Z, Shangguan D & Liu J (2006) High temperature aging study of intermetallic compound formation of Sn-3.5 Ag and Sn-4.0Ag-0.5Cu solders on electroless Ni(P) metallization. Journal of Alloys Compounds 425(1-2): 191 - 199.

82. Sundelin JJ, Nurmi ST, Lepistö TK & Ristolainen EO (2006) Microstructure, creep properties, and failure mechanisms of SnAgCu solder joints. Journal of Electronic Materials 35(7): 1600 - 1606.

83. Suh D, Kim, DW, Liu P, Kim H, Weninger JA, Kumar CM, Prasad A, Grimsley BW & Tejada HB (2007) Effects of Ag content on fracture resistance of Sn-Ag-Cu lead-free solders under high-strain rate conditions. Materials Science and Engineering A 460-461: 595 - 603.

84. Vuorinen V, Laurila T, Yu H & Kivilahti JK (2006) Phase formation between lead-free Sn-Ag-Cu solder and Ni(P)/Au finishes. Journal of Applied Physics 99(2): 3530 - 3536.

85. Chun H-S, Yoon J-W & Jung S-B (2007) Solid-state interfacial reactions between Sn-3.5Ag-0.7Cu solder and electroless Ni-immersion Au substrate during high temperature storage test. Journal of Alloys Compounds 439(1-2): 91 - 96.

86. Vuorinen V, Yu H, Laurila T & Kivilahti JK (2008) Formation of intermetallic compounds between liquid Sn and various $CuNi_x$ metallizations. Journal of Electronic Materials 37(6): 792 - 805.

87. Laurila T, Vuorinen V, Mattila T & Kivilahti JK (2005) Analysis of the redeposition of AuSn4 on Ni/Au contact pads when using SnPbAg, SnAg, and SnAgCu solders. Journal of Electronic Materials 34(1): 103 - 111.

88. Kao S-T & Duh J-G (2005) Interfacial reactions and compound formation of Sn-Ag-Cu solders by mechanical alloying on electroless Ni-P/Cu under bump metallization. Journal of Electronic Materials 34(8): 1129 - 1134.

89. Sharif A & Chan YC (2005) Interfacial reactions on electrolytic Ni and electroless Ni(P) metallization with Sn–In–Ag–Cu solder. Journal of Alloys Compounds 393(1-2): 135 - 140.

90. Islam MN, Chan YC, Sharif A & Rizvi MJ (2005) Effect of 9 wt. % In addition to Sn3.5Ag0.5Cu solder on the interfacial reaction with the Au/NiP metallization on Cu pads. Journal of Alloys Compounds 396(1-2): 217 - 223.

91. Islam MN & Chan YC (2005) Interfacial reactions of Cu-containing lead-free solders with Au/NiP metallization. Journal of Electronic Materials 34(5): 662 - 669.

92. Sharif A & Chan YC (2006) Liquid and solid state interfacial reactions of Sn-Ag-Cu and Sn–In–Ag–Cu solders with Ni-P under bump metallization. Thin Solid Films 504(1-2): 431 - 435.

93. Matin MA, Vellinga WP & Geers MGD (2006) Microstructure evolution in a Pb-free solder alloy during mechanical fatigue. Materials Science and Engineering A 431(1-2): 166 -174.

94. Korhonen T-MK, Lehman LP, Korhonen MA & Hendersson DW (2007) Isothermal fatigue behavior of the near-eutectic Sn-Ag-Cu alloy between –25 °C and 125 °C. Journal of Electronic Materials 36(2): 173 - 178.

95. Matin MA, Vellinga WP & Geers MGD (2007) Thermomechanical fatigue evolution in SAC solder joints. Materials Science and Engineering A 445-446(1): 73 -85.

96. Park S, Dhakal R, Lehman L & Cotts E (2007) Measurements of deformations in SnAgCu solder interconnects under in situ thermal loading. Acta Materialia 55(9): 3253 - 3260.

97. Lauro P, Kang SK, Choi WK & Shih D-Y (2003) Effects of mechanical deformation and annealing on the microstructure and hardness of Pb-free solders. Journal of Electronic Materials 32(12): 1432 - 1440.

98. Vianco PT, Rejent JA & Kilgo AC (2003). Time-independent mechanical and physical properties of the ternary 95.5Sn-3.9Ag-0.6Cu solder. Journal of Electronic Materials 32(3): 142 - 151.

99. Terashima S, Tanaka M & Tatsumi K (2008). Thermal fatigue properties and grain boundary character distribution in Sn-xAg-0.5Cu (x=1, 1.2 and 3) lead free solder interconnects. Science and Technology of Welding and Joining 13(1): 60 - 65.

100. Terashima S, Kohno T, Mizusawa A, Arai K, Okada O, Wakabayashi T, Tanaka M & Tatsumi K (2009). Improvement of thermal fatigue properties of Sn-Ag-Cu lead-free solder interconnects on Casio's wafer-level packages based on morphology and grain boundary character. Journal of Electronic Materials 38(1): 33 - 38.

101. Gong J, Conway PP, Liu C & Silberschmidt VV (2009) Journal of Electronic Materials 38(12): 2429 - 2435.

102. Schubert A, Dudek R, Döring R, Walter H, Auerswald E, Gollhardt A & Michel B (2002) Thermomechanical reliability of lead-free solder interconnections. In: Proceeding of the 8th International Symposium on Advanced Packaging Materials, Braselton, USA: 90 - 96.

103. Guidelines for accelerated reliability testing of surface mount solder attachments. IPC-SM-785, 1992.

104. Zhao J, Mutoh Y, Miyashita Y & Mannan SL (2002) Fatigue crack-growth behavior of Sn-Ag-Cu and Sn-Ag-Cu-Bi lead-free solders. Journal of Electronic Materials 31(8): 879 - 886.

105. Johannessen R, Oldervoll F, Kristiansen H, Tyldum H, Nguyen H-V & Aasmundtveit K (2009) Investigation of compliant interconnect for ball grid array (BGA). In: Proceedings of the European Microelectronics and Packaging Conference & Exhibition, Rimini, Italy: 1 - 6.

106. Chen T & Dutta I (2008) Effect of Ag and Cu concentrations on the creep behavior of Sn-based solders. Journal of Electronic Materials 37(3): 347 - 354.

107. Ollivier PJ, Wang Y & Needes CR Improvements in the thermal-cycled adhesion of co-fired soldered conductors on LTCC substrates. Available from: http://www2.dupont.com/MCM/en_US/PDF/techpapers/ThermalCycledAdhesion_of_ CofiredSoldered-Conductors_on_LTCC.pdf

108. Bangali J, Rane S, Phatak G & Gangal S (2008) Silver thick film pastes for low temperature co-fired ceramics: impact of glass frit variation. Soldering & Surface Mount Technology 20(3): 41 - 46.

109. Klein M, Oppermann H, Behnke S, Halser K, Aschenbrenner R & Reichl H (2002) Characterisation of plastic core solder balls for BGA and flip chip applications. In: Proceedings of IMAPS Nordic Conference, Stockholm, Sweden: 157 - 162.

110. Loeffler M (2006) Polymer-core solder balls: An alternative to solid solder balls?. Available: http://www.highbeam.com/ CircuiTree/publications.aspx?date=200606

111. Putaala J, Kangasvieri T, Nousiainen O, Jantunen H & Moilanen M (2008) Detection of thermal cycling-induced failures in RF/microwave BGA assemblies. IEEE Transactions on Electronics Packaging Manufacturing 31(3): 240-247.

112. Yoon SW & Park IS (2001) CSP board level reliability testing of Pb-free Sn-Ag-x (x=Cu, In) and polymer-core solder ball. In: Proceedings of Pan Pacific Microelectronics Symposium, Kauai, Hawaii, USA: 29 - 37.

113. Wei Z & Kuan LB (2003) Enhancing solder joint fatigue life for ball grid array packages. In: Proceedings of the 5th Electronics Packaging Technology Conference, Singapore: 701 - 706.

114. Pienimaa SK, Miettinen J & Ristolainen E (2004) Stacked modular package. IEEE Transactions on Advanced Packaging 27(3): 461 - 466.

115. Plumbridge WJ, Gagg CR & Peters S (2001) The creep of lead-free solders at elevated temperatures. Journal of Electronic Materials 30(9): 1178 - 1183.

116. Wade N, Wu K, Kunii J, Yamada S & Miyahara K (2001) Effects of Cu, Ag and Sb on the creep-rupture strength of lead-free solder alloys. Journal of Electronic Materials 30(9): 1228 - 1231.

117. Wiese S & Wolter K-J. (2007) Creep of thermally aged SnAgCu-solder joints. Microelectronics Reliability 47(2-3): 223 - 232.

118. Shirley DR, Ghorbani HR & Spelt JK (2008) Effect of primary creep and plasticity in the modelling of thermal fatigue of SnPb and SnAgCu solder joints. Microelectronics Reliability 48(3): 455 - 470.

119. Andersson C, Vandevelde B, Noritake C, Sun P, Tegehall PE, Andersson DR, Wetter G & Liu J (2009). Thermal cycling of lead-free Sn-3.8-0.7Cu 388PBGA packages. Soldering & Surface Mount Technology 21(2): 28 - 38.

120. Heraeus datasheet. LTCC tape CT 800. Available from: http://www.heraeus-thickfilm.com /media/webmedia_local/media /datasheets/ltccmaterials/CT_800_en.pdf

121. Heraeus technical information. Design guidelines for LTCC: Heralock HL 2000 materials system. Available from: http://www.seaceramics.com/Download /Design%20Guides/HL2KDG.pdf

122. Sato S, Shimizu N, Matsuda S, Uegaki S & Ninomiya S (1997) 2nd level interconnect reliability of ceramic area array packages. Available from: http://www.twinstar-tech.com/doc/KyoceraCBGAReport.pdf (accessed 6 May 2010).

123. Sigliano R (2002) HiTCE ceramics: Bridging the gap between ceramics and organic packaging. Advancing Microelectronics 29(5): 12 - 14.

124. Syed A & Doty M (1999) Are we over designing for solder joint reliability? Field vs. accelerated conditions, realistic vs. specified requirements. In: Proceedings of the 1999 Electronic Components and Technology Conference, San Diego, USA: 111 - 117.

125. Kangasvieri T (2008) Surface-mounTable LTCC-SiP module approach for reliable RF and millimeter-wave packaging. PhD thesis, University of Oulu, Department of Electrical and Information Engineering.

126. Needes CRS & Brown JP (1989) The thermal-cycled adhesion strength of soldered thick film silver-bearing conductors. In: Proceedings of ISHM '89, Baltimore, USA: 211 - 219.

127. Voutilainen J, Putaala J, Moilanen M & Jantunen H (2009) A prognostic method for the embedded failure monitoring of solder interconnections with 1149.4 test bus architecture. Microelectronics Journal 40(7): 1069 - 1080.

128. Dr. Kangasvieri's private communication with vendor.

129. Puttlitz KJ (2004) Overview of lead-free solder issues including selection. In: Puttlitz KJ, Stalter KA (eds.). Handbook of lead-free solder technology for microelectronics assemblies, Mercel Dekker New York, USA.